Solar Energy Potential Assessment on Rooftops and Facades in Large Built Environments Based on LiDAR Data, Image Processing, and Cloud Computing. Methodological Background, Application, and Validation in Geneva (Solar Cadaster)

Desthieux, Gilles; Carneiro, Claudio; Camponovo, Reto; Ineichen, Pierre; Morello, Eugenio; Boulmier, Anthony; Abdennadher, Nabil; Dervey, Sébastien; Ellert, Christoph

How to cite

DESTHIEUX, Gilles et al. Solar Energy Potential Assessment on Rooftops and Facades in Large Built Environments Based on LiDAR Data, Image Processing, and Cloud Computing. Methodological Background, Application, and Validation in Geneva (Solar Cadaster). In: Frontiers in Built Environment, 2018, vol. 4, n° 14. doi: 10.3389/fbuil.2018.00014

This publication URL: https://archive-ouverte.unige.ch/unige:103199
Publication DOI: 10.3389/fbuil.2018.00014

frontiers in Built Environment

METHODS
published: 22 March 2018
doi: 10.3389/fbuil.2018.00014

Solar Energy Potential Assessment on Rooftops and Facades in Large Built Environments Based on LiDAR Data, Image Processing, and Cloud Computing. Methodological Background, Application, and Validation in Geneva (Solar Cadaster)

Gilles Desthieux[1], Claudio Carneiro[1], Reto Camponovo[1], Pierre Ineichen[2], Eugenio Morello[3], Anthony Boulmier[4], Nabil Abdennadher[4], Sébastien Dervey[5] and Christoph Ellert[5]*

[1] Haute école du paysage d'ingénierie et d'architecture de Genève (hepia), Institute for Landscaping Architecture Construction and Territory (inPACT), University of Applied Sciences Western Switzerland, Geneva, Switzerland, [2] Energy Systems, University of Geneva, Geneva, Switzerland, [3] Laboratorio di Simulazione Urbana "Fausto Curti", Politecnico di Milano, Milano, Italy, [4] Haute école du paysage d'ingénierie et d'architecture de Genève (hepia), Large-Scale Distributed Systems Research Group (lsds-rg), University of Applied Sciences Western Switzerland, Geneva, Switzerland, [5] Institute of System Engineering, University of Applied Sciences (HESSO-Valais-Wallis), Sion, Switzerland

OPEN ACCESS

Edited by:
Vahid Nik,
Lund University, Sweden

Reviewed by:
Graziano Salvalai,
Politecnico di Milano, Italy
Silvia Coccolo,
École Polytechnique Fédérale de Lausanne, Switzerland

***Correspondence:**
Gilles Desthieux
gilles.desthieux@hesge.ch

Specialty section:
This article was submitted to Sustainable Design and Construction, a section of the journal Frontiers in Built Environment

Received: *19 November 2017*
Accepted: *22 February 2018*
Published: *22 March 2018*

Citation:
Desthieux G, Carneiro C, Camponovo R, Ineichen P, Morello E, Boulmier A, Abdennadher N, Dervey S and Ellert C (2018) Solar Energy Potential Assessment on Rooftops and Facades in Large Built Environments Based on LiDAR Data, Image Processing, and Cloud Computing. Methodological Background, Application, and Validation in Geneva (Solar Cadaster). Front. Built Environ. 4:14. doi: 10.3389/fbuil.2018.00014

The paper presents the core methodology for assessing solar radiation and energy production on building rooftops and vertical facades (still rarely considered) of the inner-city. This integrated tool is based on the use of LiDAR, 2D and 3D cadastral data. Together with solar radiation and astronomical models, it calculates the global irradiance for a set of points located on roofs, ground, and facades. Although the tool takes simultaneously roofs, ground, and facades, different methods of shadow casting are applied. Shadow casting on rooftops is based on image processing techniques. On the other hand, the assessment on facade involves first to create and interpolate points along the facades and then to implement a point-by-point shadow casting routine. The paper is structured in five parts: (i) state of the art on the use of 3D GIS and automated processes in assessing solar radiation in the built environment, (ii) overview on the methodological framework used in the paper, (iii) detailed presentation of the method proposed for solar modeling and shadow casting, in particular by introducing an innovative approach for modeling the sky view factor (SVF), (iv) demonstration of the solar model introduced in this paper through applications in Geneva's building roofs (solar cadaster) and facades, (v) validation of the solar model in some Geneva's spots, focusing especially on two distinct comparisons: solar model versus fisheye catchments on partially inclined surfaces (roof component); solar model versus photovoltaic simulation tool PVSyst on vertical surfaces (facades). Concerning the roof component, validation results emphasize global sensitivity related to the density of light sources on the sky vault to model the SVF. The low dense sky model with 145 light sources gives satisfying results, especially when processing solar cadasters in large urban areas, thus allowing to save computation time.

In the case of building facades, introducing weighting factor in SVF calculation leads to outputs close to those obtained by PVSyst. Such good validation results make the proposed model a reliable tool to: (i) automatically process solar cadaster on building rooftops and facades at large urban scales and (ii) support solar energy planning and energy transition policies.

Keywords: urban solar cadaster, shadow casting, sky view factor, energy management, 3D-urban digital models, cloud computing

INTRODUCTION

The increasing attention given to environmental issues during the last two decades in urban studies has opened up many questions about the way territory planners should manage the design process. In fact, numerous authors and architects are convinced that cities play a leading role in controlling sustainability. This goal may be achieved through: (i) strategies for redefining more efficient cities in terms of energy performance and environmental quality, already a main focus of many European cities (Owen Lewis et al., 2013) and (ii) a broad debate around the promotion of more sustainable cities (Ritchie and Randall, 2009).

Nowadays, the stress on the use and control of solar radiation on the urban fabric has become extremely relevant due to the increasing prominence of the resulting energy-saving repercussions. In fact, an increasing significance is given to public policies related to the exploitation of renewable energy through solar energy as a major lever for energy transition. In 2014, EU countries have agreed on a new 2030 Framework for climate and energy, including EU-wide targets and policy objectives for the period between 2020 and 2030. One of the targets involves reaching at least a 27% share of renewable energy consumption (European Commission, 2014). In 2011, the Federal Council and Parliament established that Switzerland is to pull out from the use of nuclear energy on a gradational basis. The existing five nuclear power plants of Switzerland are to be withdrawn when they achieve the end of their harmless service life, and will not be substituted by new ones. As a consequence of this choice and several other thoughtful changes that have been perceived for a number of years, the Swiss energy system will have need of succeeding reorganization until 2050. As a result of this, the Swiss Federal Council has settled a long-term energy policy ("Energy Strategy 2050") built around the massive development of renewable energy sources in order to supply the energy demand in electricity, hence taking the place of nuclear energy (Conseil Fédéral, 2013).

However, if the development of solar energy is particular relevant in cities that consume the major part of energy demand, dense areas limit the incoming sunlight and the deployment of urban solar power plants. Therefore, it is essential to make available tools that model the solar energy accessibility in the urban fabric (Freitas et al., 2015). Today's availability of 3D information about cities offers the possibility for such modeling, involving a whole procedure from data acquisition from Airborne Laser Scanning, also called Light Detection and Ranging (LiDAR), to the environmental analysis through the image processing of digital urban models. Building roofs, but also potential usable surfaces like car-port or highways roofs and walls are considered for potential energy production. Vertical or building facades, which are particularly interesting for the production of solar energy during the winter months, are becoming more and more promising through the improvement of solar panel efficiency and the innovative concepts of Nearly Zero-Energy Buildings (nZEB) and Building Integrated PhotoVoltaics (BiPV) concepts. In order to achieve the nZEB standard, it is now largely admitted that a significant increase in energy efficiency of existing buildings cannot be simply achieved by working on building's envelope but also through the integration of high performance systems like those based on BiPV (Marszal et al., 2011; Kamel et al., 2015; Aste et al., 2017). However, facade modeling for solar analysis is not as explored as for roofs, since it requires much more complex tools based on 3D GIS data.

The work presented in this article has been partially published, but only in the initial stage of the solar cadaster implemented in Geneva and considering only solar accessibility on horizontal surfaces (Carneiro et al., 2009; Desthieux et al., 2011, 2014, 2018). The paper aims at giving a complete and updated view of the work, also including recent refining in the solar algorithms used, integration of the roof and facades components in a single tool, improvement of computation through cloud computing, and application and validation of the tool in Geneva's case-study areas.

This integrated tool is based on the use of LiDAR, 2D and 3D cadastral data. Together with solar radiation and solar astronomical models it calculates the global solar irradiance for a set of points located on roofs, ground, and facades. Although the tool takes simultaneously roofs, ground, and facades, the method applied for roofs and ground processing is different from the one applied for facades processing.

After the state of the art, the following sections present the synoptic view of the methodology and detail the steps and theoretical approaches used for shadowing and solar irradiation calculation (**Figure 1**). It illustrates then the application of the tool and presents the results of validation using measured data in Geneva's case-study areas.

STATE OF THE ART

From Building to Urban Scale and from Computer Aided-Design (CAD) to GIS Tools

The investigation of solar radiation environmental analysis is not new and there are several tools that allow the calculation

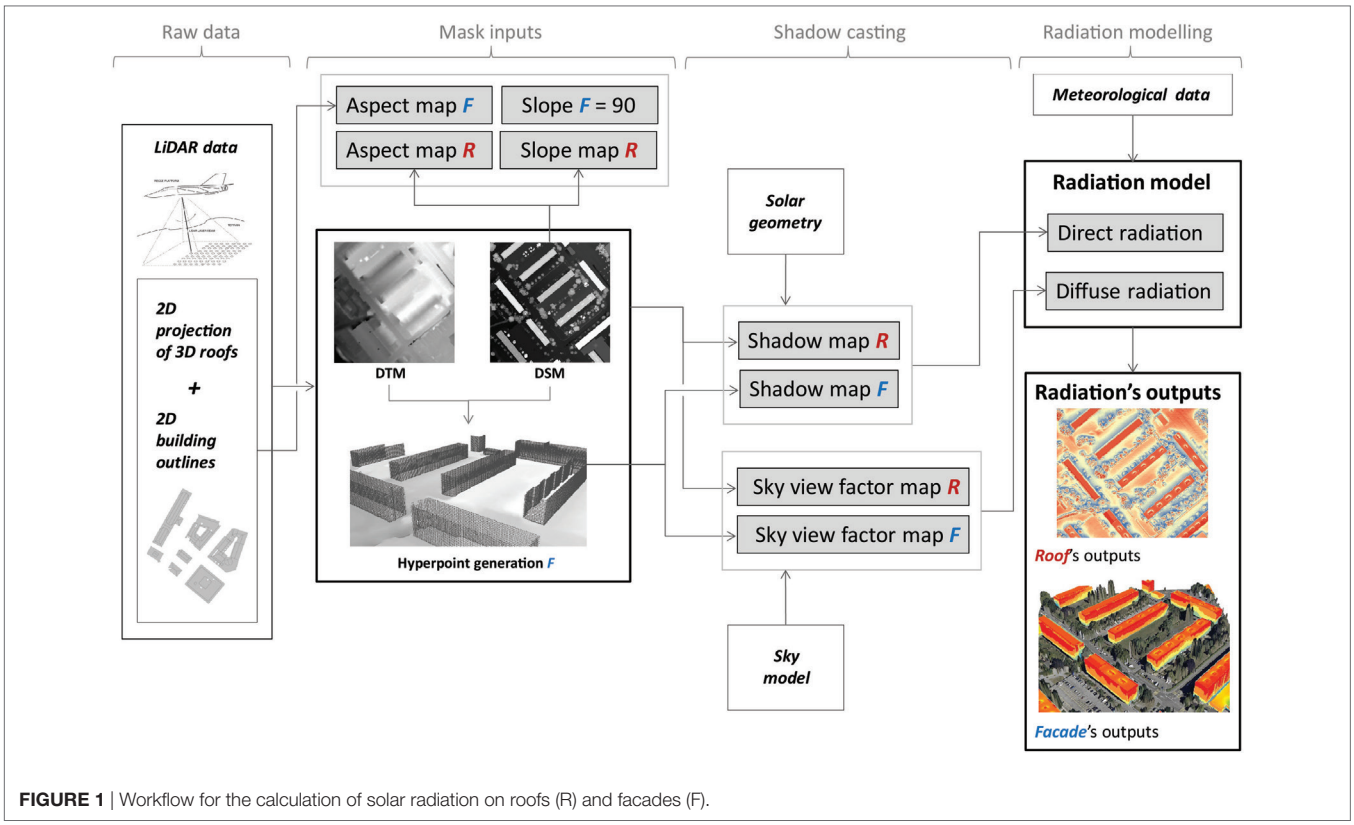

FIGURE 1 | Workflow for the calculation of solar radiation on roofs (R) and facades (F).

of radiation performance of buildings, either at the micro-scale of architecture (environmental performance software) or at the macro-scale of urban area and landscape (GIS tools).

In the micro-scale domain (architecture, urbanism), many tools are based on CAD and consist in simulating solar access: (i) RADIANCE lighting simulation model (Compagnon, 2004), (ii) TOWNSCOPE II (Teller and Azar, 2001), (iii) SOLENE (Miguet and Groleau, 2002), and (iv) other works presented by Ward (1994), Robinson et al. (2005), and Erdelyi et al. (2014). However, due to limitation on computational power, those tools demonstrate to be prohibitive if we have to undergo larger parts of the urban fabric. Moreover, even with forceful means, the degree of accuracy would be nevertheless too high and superfluous for the purposes of analysis at larger scales of the city.

For this reason, almost 20 years ago, Batty and Longley (1994) already stressed the need to couple such CAD tools with 3D GIS so as to: (i) include processing of large amount of data and spatial analysis systems and (ii) provide automatic or systematic environmental analysis on urban area, like solar radiation calculation.

Solar Potential Urban-Oriented Models Based on 2.5D and 3D GIS Tools

Freitas et al. (2015) made a very complete state-of-the-art review of the different approaches and tools to model the solar potential in the urban environment. The paper distinguishes several concepts and numerical methods, as core tools for the aforesaid type of solar modeling: (i) urban-oriented models involving CAD plugin-based models that can be combined with spatial data and (ii) GIS-based models. In the following, we will focus on the latter based on either numerical (LiDAR) or vector data.

Several approaches for modeling the solar potential at urban large scale using LiDAR data were already developed. Indeed, classified LiDAR data points allow to automatically construct an enhanced Digital Surface Model (DSM) in a step-by-step basis, with information about ground, buildings, and vegetation (Carneiro, 2011). Such DSM based on LiDAR data enables then fast, automatic, and systematic calculation of various indicators at large scales of the city, such as building morphology and solar radiation.

2.5D DSM derived from LiDAR data and raster-based calculation techniques are commonly used for solar radiation assessment at the urban scale (Carneiro, 2011; Jakubiec and Reinhart, 2013; Redweik et al., 2013; Verso et al., 2015). In this regard, among different tools and approaches, we mention two of them among the most recent: (i) the Solar Energy on Building Envelopes (SEBE) model (Lindberg et al., 2015) and (ii) the SOL model (Redweik et al., 2013). Both estimate irradiance on roofs and building walls using high resolution DSMs, but differently managing hourly shadow masks.

All these methods implement the usual solar geometry formulae on tilted surfaces, considering the components of beam, diffuse, and reflected irradiation. Different approaches

of the diffuse component are used, in general according to the model of anisotropy of Hay and Davis (Hay, 1979) or Perez et al. (1990). Shadow casting routines vary according to the approaches used. Some of them use the hillshade approach proposed by Verso et al. (2015). Another option commonly used is the routine developed by Ratti and Richens (1999, 2004). The latter is used by SEBE and SOL tools as well as in the method described in the present article, but refining the algorithms as presented in Section "Application of Shadow Casting to Solar Diffuse Component (SVF) and Choice of an Appropriate Sky Vault Model."

Due to the limitation of the 2.5D approach that does not truly represent the building walls, most of the proposed models limit themselves to the analysis of horizontal and tilted not vertical surfaces. However, some of the models presented above are able to derive 3D irradiation of the wall from the 2.5D raster modeling approach. This is in particular the case of the SOL model that interpolates the so-called "hyper" points or facades segments from the edges of the roof to the ground (Redweik et al., 2013). The integrated tool described in the present paper applies a similar procedure, but improving systematic facade delimitation and time computation as discussed further.

The main drawback of such tools for deriving 3D information on wall from a 2.5D raster model is that no information can be obtained on some details of the facades, such as windows or balconies, which are important for any solar panel installation.

Hence, the methods and tools presented in this article can be intended just as one tile of a larger mosaic aiming at quantifying environmental parameters at the urban scale. Using the capability of LiDAR data for constructing an accurate 2.5-DSM, different tools are then applied in order to calculate solar radiation incident on the urban fabric, as underlined in this article through Geneva's case-study areas Moreover, it is worth mentioning that most of the results obtained in past studies related to solar analysis in urban areas are represented using only a 2D GIS environment. In this article, we intend to move further by presenting this type of results in a 3D GIS environment.

METHODOLOGICAL FRAMEWORK

First of all a global overview is given on the approach and method used to compute solar radiation on horizontal and titled surfaces (roofs) and vertical surfaces or facades (see Overview). Then, the main theoretical concepts used and developed in our method related to solar radiation (see Solar Irradiation Calculation) and shadow casting routine (see Shadow Casting Routine), are introduced.

Overview

Workflow for the Calculation of Solar Irradiance on Roofs and Facades

Our method uses a hybrid approach distinguishing: (i) raw data, (ii) input data preparation for modeling, (iii) shadow casting, and (iv) solar model processing for solar radiation calculation on roofs and facades.

Raw Data for Digital Terrain Model (DTM) and DSM Construction

The following raw data are used in order to construct DTM and DSM:

- LiDAR data used has a density of 15 to 20 points/m^2, a planimetric accuracy of 15 cm and an altimetric accuracy of 10 cm. Classification based on specific algorithms enables to attribute LiDAR points either to buildings, terrain, or vegetation classes (Axelsson, 1999).
- The terrain is interpolated from LiDAR classified;
- 2D projections of 3D vector roof outlines are used to construct a so-called here DSM of roofs, also including vegetation;
- 3D vector roof footprints are used to construct a so-called here DSM of facades, also including vegetation;
- 2D vector building outlines are used to enhance the DSM of facades constructed in the previous step.

Mask Inputs Production for Solar Modeling

From raw data, DTM, DSM of roofs and facades are built along with further inputs (aspect, slope, hyperpoints):

- 2.5D DTM and DSM: spatial interpolation techniques (e.g., triangulated irregular network) are used to construct a rectangular array of z values with specific resolution. This type of models are commonly derived from irregularly spaced x, y, z LiDAR data points (see Raw Data for DTM and DSM Construction).
- It is relevant to construct two main independent DSM for roofs and facades, respectively, because, in many cases, the building outlines (that determine the facades position) do not necessarily represent the outline of the building roof.
- For the calculation of solar analysis on roofs, DSM altitude values are uniquely interpolated from classified LiDAR data. The use of 2D projections of 3D vector roof outlines allows to interpolate and correctly delimitate existing roofs. The DSM is then constructed in a step-by-step basis: DTM (from LiDAR data) + normalized DSM of roofs (from LiDAR and 3D vector data) + normalized DSM of vegetation (from LiDAR data).
- For the calculation of solar radiation on *facades*, only pixels of the DSM corresponding to terrain and vegetation are interpolated from classified LiDAR data. The reason is that altitude values of the DSM constructed only from LiDAR data quite often are random along zones of discontinuity, such as building facades. Hence, another data source is used to interpolate regular height values on roofs: 3D vector roof footprints. Finally, 2D vector building outlines are also used to precisely "cut" roofs along touching facades, thus enhancing the DSM of facades constructed in a step-by-step basis: DTM (from LiDAR data) + normalized DSM of roofs delimited to facades (from 2D and 3D vector data) + normalized DSM of vegetation (from LiDAR data).
- The image processing of the DSM of roofs allows producing different maps, such as *height values*, *slope*, and *aspect*, all needed for the solar direct and diffuse irradiation calculation. The aspect's mask of facades is rasterized from the aspect's values of the 2D building outlines. The slope's mask of facades has logically a constant value of 90°.

- Furthermore, as the 2.5D approach based on DSM does not allow dealing with facades, it is further necessary to add the third dimension in order to model the facades. The "*hyperpoint*" approach is thus introduced here, similarly to Redweik et al. (2013), as highlighted in **Figure 2**. First of all, building outline points are generated from 2D vector data of building outlines. Then, from each point of a given height at the top of the building, hyperpoints are generated every 1 m along the facade until reaching the height of the ground defined by the DTM. Finally, it is worth mentioning that in our research we propose an innovative and more truthful procedure for the detection and calculation of orientation of each building facade, which is based on the use of vector building outlines (each of them representing a single facade). Redweik et al. (2013) proposed another method for detection of building facades based only on the analysis of pixels of the DSM with a slope higher than 72°. Main disadvantage of this method is that the delimitation of facade is not accurate: local shadowing effects are created when facades are not straight. Moreover, it is not suitable for urban areas presenting tall vegetation because it is not possible to distinguish which pixels with slope higher than 72° belong to buildings or trees.

Shadow Casting and Solar Radiation Modeling

In the case of the presented tool, solar radiation modeling on DSM roof pixels and facade hyperpoints is encoded using open source Java programming language. It can be run either for roof or facades separately or for both applications at the same time.

The process follows the given steps:

- Shadow casting routine is applied to direct hourly shading calculation based on DSM and sun positions as input data (see Application of Shadow Casting to Solar Beam Component).
- Shadow casting routine is applied to sky view factor (SVF) calculation based on DSM and the sky subdivision model of 580 light sources (see Application of Shadow Casting to Solar Diffuse Component (SVF) and Choice of an Appropriate Sky Vault Model).
- For every DSM pixels and facade hyperpoints, computation of hourly solar radiation is based on: (i) statistical meteorological data of the studied area (hourly global, diffuse and direct solar radiation on flat surface), (ii) shadow casting outputs (SVF and direct), and (iii) slope and aspect of the pixel (based on DSM). As a result, monthly, and yearly solar radiation values are calculated for each pixel of the outputted raster grids or facade hyperpoints.
- Post-processing: calculation of statistics and indicators (energy production, costs of installation, CO_2 savings, etc.) on roofs and facades, in the framework of city solar cadasters (see Solar Cadaster in Geneva's Building Roofs).

Solar Irradiation Calculation

Global Approach

The usual solar geometry formula, given below, allows deriving *hourly* global irradiation on inclined surface ($I_{g\beta\gamma}$) from the direct or beam ($I_{b\beta\gamma}$), diffuse (I_S) and ground reflected (I_r) components for every orientation γ (or aspect) and inclination β (or slope) of surfaces (Iqbal, 1983):

$$I_{g\beta\gamma} = I_{b\beta\gamma} * S_b + I_S * f(S_d, S_b) + I_r. \quad (1)$$

To the main components of the global irradiation (direct $I_{b\beta\gamma}$ and diffuse I_S), the following shadowing factors are applied:

- Shadowing (S_b) on the beam component and the circumsolar (anisotropic) part of the diffuse component at a given hour. The value is 0 if a given roof or facade point is shaded at given hour or 1 if the point is not shaded.
- Shadowing on the isotropic part of the diffuse component (S_d) [0, 1]: the calculation of the SVF evaluates the reduction of the sky visibility from a roof or facade point due to obstacles in the surrounding environment. It is thus not time-dependent. Its values range between 0 and 1.

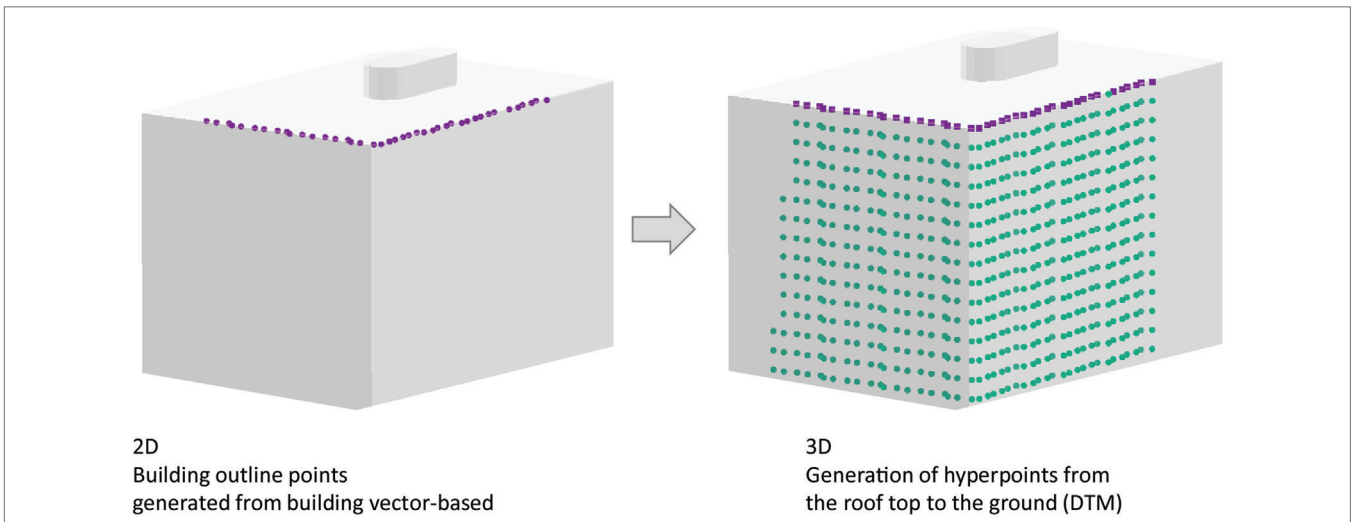

FIGURE 2 | Generation of facades' "hyperpoints" using 2D vector data of building outlines.

- $f(S_d, S_b)$ is a function of both shadowing factors on beam and diffuse components, as specified in Section "Final Irradiation Formula Applying Shadowing Factors to Solar Components."

For the computation of such shadowing factors, a shadow casting routine is applied to the input masks of roofs and facades. More details on shadow analysis and factors are given in Section "Shadow Casting Routine."

Meteorological Data Sources

The solar irradiation data used was sourced from METENORM®. The latter is a meteorological reference incorporating a catalog of meteorological data and calculation procedures for several locations in the world. This database offers, among other features, average data on global, beam and diffuse radiation incident on horizontal surface, for a given time period and scale. From the monthly values (station data), METEONORM® calculates hourly values of all these parameters using a stochastic model. The resulting time series correspond to "typical years." The used version, (7.1), provides statistical data of a typical year that corresponds to the period 1990–2010 for a given location. However, calculating irradiation for each hour of a typical year and for each pixel of a high resolution DSM model would result in prohibitive time of calculation. Consequently, solar irradiation dataset is reduced by averaging hourly values for each month. The yearly dataset contains thus 288 (24 h × 12 months) hourly values instead of 8,760. If we consider the sunny hours from sunrise to sunset, the dataset is reduced to 154 hourly values in the case of the studied area of Geneva (latitude 46.2°N). The solar geometry taken into account corresponds to the day considered to be the mostly representative of each month, which is usually close to the day 15 (Klein, 1977). This data reduction method is mainly used by scientists to validate solar radiation estimation models that are used in photovoltaic power plants planning (e.g., Maleki et al., 2017).

Diffuse Component: Choice of the Suitable Anisotropic Sky Model

In many instances, models attempting to account for diffuse radiation anisotropy have demonstrated to be better than the isotropic model. The most successful and common models are those proposed by Perez et al. (1986, 1987, 1990), and Hay (1979). In a comparative study of several models, Perez et al. (1986) showed that the Perez model achieves the most reliable results with regards to the measured diffuse radiation in different parts of the world.

However, as explained above, the solar model implemented here uses a reduced solar irradiation dataset by averaging hourly values for each month. If the reference anisotropic model of Perez is particularly addressed for very accurate time scale (minute or hour), authors have verified that the Hay model is more suitable when using average hourly values by month (Carneiro, 2011). Indeed, authors made a sensitivity analysis and a theoretical comparison between average and not average hourly values considering different slopes and orientations on a monthly and yearly basis. Main conclusion is that gaps are in general low (less than 1%), except for northern orientation and high slope (up to 3.6% for North and vertical surface). On the other hand, Perez model shows higher gaps for southern orientation (up to 5.2% for South and vertical surface), which is less acceptable, particularly in the perspective of installing near-south-oriented surfaces with solar panels.

Shadow Casting Routine

Global Approach

This section explains the Shadow casting algorithm used for shadowing on solar beam (direct) and for SVF (isotropic diffuse) components. Shadow casting algorithm calculates the shadow map from a given DSM according to a given light source defined by its position (azimuth and altitude).

The purpose of the algorithm is to assess, for each point (pixel) P that belongs to the DSM, which other point P_0 is shading according to a given light/signal source, as showed in **Figure 3**. When the light source (i.e., the sun) is in position 1, H_1 is higher than P_1, thus P_0 is lighted. On the other hand, when the light source is in position 2, $H_{2'}$ is lower than P_1 (i.e., the tree), thus P_0 is shaded. In the same manner, in light source position 3, P_0 is shaded by both the building (P_2) and the three (P_1), H_3 being lower that P_2, H_2, and H_3, being lower than P_1.

Therefore, the algorithm can be formalized by the following equation:

$$S_l(P_0) = !\bigvee_{m=1}^{MSP}(P_m > H_{l\,m}), \tag{2}$$

$S_l(P_0)$ is a Boolean value (0 for shaded, 1 otherwise) that represents the shading of each point P_0 for a given light source l. As stated above, $S_l(P_0)$ is equal to 0 if P_0 is shaded, 1 otherwise. $\bigvee$ Symbol represents a logical OR. MSP is the maximum shadow propagation threshold, hence representing the maximum size of a shadow for the given DSM.

The shadow casting algorithm was implemented by Ratti and Richens (1999, 2004) based on a *matrix approach*. It consists in processing the image (DSM) and calculting shadow for each pixel of the image, as follow: for a given light source and a given point *P*, the algorithm proceeds in the direction of the light source and checks if the encountered points (buildings, trees, obstacles) hide *P* (**Figure 3**). Therefore, for each pixel that belongs to a DSM, this algorithm applies an iterative search of an obstacle that hides *P* inside its neighborhood.

For instance, this matrix approach is used for computing shadow casting on a DSM in the case of solar radiation analysis on roof buildings.

As explained in Section "Mask Inputs Production for Solar Modeling," facades are modeled as sets of hyperpoints (*point-by-point approach*) before applying solar radiation analysis. The principle is the same as the matrix approach, except for the following points: (i) the shadow is casted on each hyperpoint of a facade (instead of pixel roof from the DSM) and (ii) the process stops immediately after the point is shaded (i.e., if at least one of its neighbor point is higher than itself). This way, the process is much faster when compared to the matrix approach, which considers all of neighbor pixels in the direction of the light source.

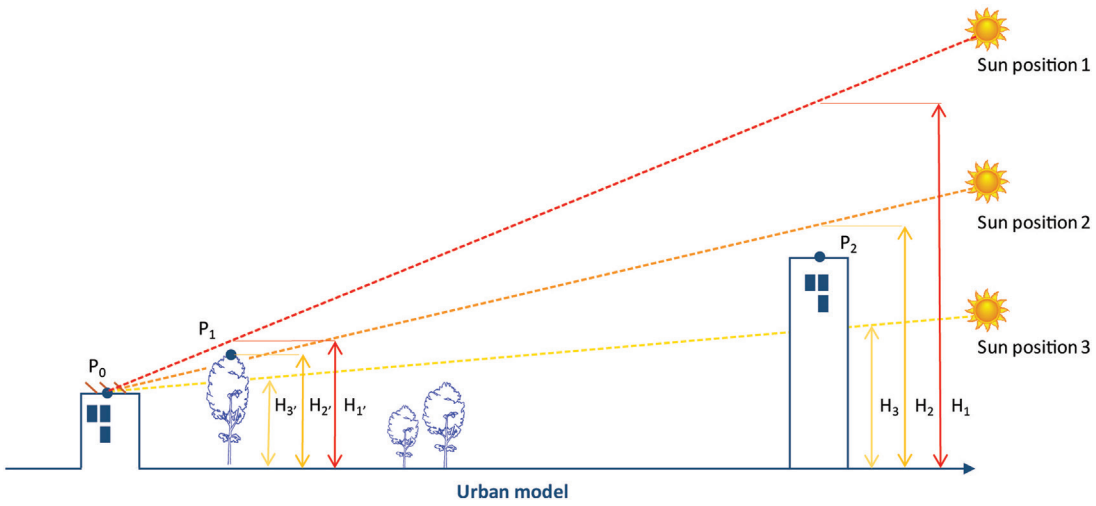

FIGURE 3 | Principle of the shadow casting algorithm, adapted with permission from ©2018 Springler (Desthieux et al., 2018).

FIGURE 4 | Calculated shadows for an area of Geneva at three times of the day (September 15).

Application of Shadow Casting to Solar Beam Component

Shadow casting routine is applied to each pixel of the DSM and at every sunny hour considering the sun position (azimuth and height) and the possible surrounding obstacles as modeled by the DSM. As given in Section "Global Approach", $S_l(P_0)$ is set to either 1 (not shaded) or 0 (shaded) and multiplied by the beam hourly irradiation value.

As illustration, **Figure 4** shows three calculated shadow maps for an area of Geneva ("Meyrin—Cité") at 9:00 a.m. (left), 12:00 a.m. (center), and 4:00 p.m. (right) on September 15.

Application of Shadow Casting to Solar Diffuse Component (SVF) and Choice of an Appropriate Sky Vault Model

At any given location, a portion of the sky vault may be obstructed by surrounding urban environment and topography, which reduces diffuse irradiance from corresponding sky directions (Dubayah and Rich, 1995). Sky obstruction can result either from "self-shadowing" by the slope itself or from adjacent terrain. Therefore, the SVF is a dimensionless parameter with values varying from 0 to 1, thus representing the fraction of visible sky on a hemisphere which lays centered over the analyzed location (Hämmerle et al., 2011).

The last author made a comparative analysis of different programs used to compute SVF, which are based on one of the following data sources: (i) support fisheye taken by picture or simulated, (ii) 3D vector-based building, (iii) DSM. These programs use different methods for weighting sky obstacles on their zenith angle. Such methods are consistent with the way of sky subdividing through a set of light sources distributed on the sky vault. Many sky subdivision strategies can be applied, such as summarized by Freitas et al. (2015). A trustworthy option, used in this work, is the uniform (equal solid angle), like the common Tregenza (1987) model with 145 light sources, triangles and equal-angular. Thus, the purpose of weighting sky image is to account for the different size of sky elements (solid angles) projected on a flat surface, depending on the angular distance from zenith (Steyn, 1980; Holmer, 2011).

The shadow casting routine (Ratti's shadowing casting routine) used in this work, introduced by Ratti and Richens (1999) and presented in Section "Global Approach," is repeated for each light source of the sky vault. At the end, the SVF output results by making the ratio between the sum of visible light sources and the total of light sources, from the point of view of a given DSM's pixel or a facade hyperpoint.

Using this routine with an equal solid angle sky model, but without weighting method, corresponds to the so-called sky angle of sky visibility and not to the SVF, as mentioned by Ratti and Richens (1999). Therefore, the latter suggest that it is appropriate to consider that light sources are distributed non-uniformly, with the density of samples being higher at the zenith than at the horizon, which corresponds to an equal-angular approach. Hence, such a non-uniform sky model indirectly introduces a "cosine" weighing factor.

In addition to the sky subdivision approach (equal-area vs equal angle), the time of computation is another important criterion. It requires using a model with not too many points, as the number of iteration proposed by Ratti's shadowing casting routine corresponds to the number of points available in the sky

vault. Yet Ratti and Richens (1999) and Redweik et al. (2013) proposed respective sky models with 1,000 or more points, such a choice may involve to prohibitive time of computation for large urban areas (>4 km²). Sensitivity analysis made by the authors on equal-angular approach showed that SVF results using up to 400 sky points were not significantly different from those using up to 1,000 points and more.

Moreover, the equal-angular approach, particularly when based on a high number of sky points, tends to overweight the near zenithal sector of the sky vault, thus overestimating the SVF final result. Therefore, we propose to implement Ratti's shadowing casting routine with *an equal solid angle sky model of 580 light sources* [centroids of solid angles of 20 milisteradian (msr)], which consists in densifying the model of Tregenza (145 solid angles of 40 msr).

This sky model is built on light source's height increment ("*annulus*") of 5° (starting from 5° and going until 89°) and on weighting factor, which is the sinus of the angle α′ defined by the light source' height relatively to the inclined surface. This choice gives more weight to light sources from the zenith than to those from the horizon, which is consistent with solar potential analysis purpose. The SVF of a given DSM pixel (P) or façade hyperpoint (P) over of a sky vault of *n* light sources is thus defined as following:

$$\mathrm{SVF}(P) = \frac{\sum_{l=1}^{n} S_l(P)\sin_l(\alpha')}{\sum_{l=1}^{n} S_l(P)\sin_l(\alpha)}. \tag{3}$$

In the numerator, the visibility of sky points is casted on the DSM pixels or facade hyperpoints using the Ratti's shadow routine. The denominator gives the maximum visibility value that occurs on flat surface. The weighting angle α is simply defined by the height of the light source from the horizontal plan and is equal to $90 - \theta_z$. In case of inclined surfaces, α′ depends on the slope of the surface and both azimuths of the light source and the inclined surface. The angle α′ is thus equal to $90° - \theta$, θ being angle of incidence of an inclined surface (DSM pixel or hyperpoint). It is a function of the zenith angle (θ_z) and azimuth of the light source (ψ), the slope (β), and azimuth (γ) of the inclined surface. It is defined by Iqbal (1983) as following:

$$\theta = a\cos[\cos\beta\cos\theta_z + \sin\beta\sin\theta_z\cos(\psi - \gamma)]. \tag{4}$$

If $90° - \theta$ is negative, it means that the light source is not visible from the point of view of the inclined surface due to its slope and azimuth (aspect), and the light source is not taken into account in the SVF balance (set to 0 for this light source).

Such weighted equal-areal model is particularly advantageous when using the DSM. Indeed, pixels' heights are not totally constant on flat surfaces and the pixels' slopes are not regular on titled surfaces. This incoherence is caused by the error margin in height (about 10–20 cm) which characterizes LiDAR data. Such irregular structure may create micro-shadowing effects between neighbor pixels. Therefore, giving less weight to low light sources close to the horizon will reduce such micro-shadowing effects. On the other hand, in the equal-angular approach with no direct weighting factor, height increments of the sky model should start higher (around 15°), which results in removing the two first "*annulus*" (5° and 10°) and alternate the sky model.

Final Irradiation Formula Applying Shadowing Factors to Solar Components

Let us first remind that the Hay model (diffuse component) has two components: the isotropic and anisotropic (circumsolar) components. The circumsolar depends on the sun position, whereas the isotropic component does not.

For reminder, the Hay model is the following (Hay, 1979; Iqbal, 1983):

$$I_s = I_d\left\{\underbrace{\frac{I_g - I_d}{I_0}r_b}_{\text{circumsolar}} + \underbrace{\frac{1}{2}(1+\cos\beta)\left[1 - \frac{I_g - I_d}{I_0}\right]}_{\text{isotropic}}\right\}. \tag{5}$$

Therefore, as exposed through Eq. 1, at any location (DSM pixel and facade hyperpoint), the hourly shadowing value related to sun position can be applied to both beam and diffuse circumsolar components. The SVF, which is not time and sun position dependent, can be applied to diffuse isotropic component only. Both hourly shadowing and SVF uses the Ratti and Richens (1999) shadow casting routine, as presented in Section "Global Approach."

However, the isotropic diffuse component already takes into account the slope (β) effect on sky visibility through the equation part 1/2*(1 + cosβ). The latter corresponds to the SVF, but only considering the slope effect. In other words, it gives the *best possible view* from a given tilted surface (the maximum sky visible being 100% on a flat surface and 50% on a vertical surface). Hence, by taking also into account the shadowing from the surrounding obstacles Hay's equation part can be replaced by the SVF as it considers both slope and shadowing effects on the reduction of the sky visibility.

The Eq. 5, taking into account shadowing effects, can be thus rewritten as follows:

$$I_s = I_d\left\{\underbrace{\frac{I_g - I_d}{I_0}r_b}_{\text{circumsolar}} + \underbrace{\mathrm{SVF}\left[1 - \frac{I_g - I_d}{I_0}\right]}_{\text{isotropic}}\right\}. \tag{6}$$

Finally, we propose to rewrite hourly global irradiation on inclined surface (with slope β from 0° to 90°), from Eq. 1, as follows:

$$I_{g\beta\gamma} = \underbrace{I_{b\beta\gamma}r_bS_b}_{\text{Beam}} + \underbrace{I_d\left\{\frac{I_g - I_d}{I_0}r_bS_b + \mathrm{SVF}\left[1 - \frac{I_g - I_d}{I_0}\right]\right\}}_{\text{Diffuse}} + \underbrace{0.5I_g a(1-\cos\beta)}_{\text{Reflected}}. \tag{7}$$

APPLICATIONS

This chapter presents some applications of the method and algorithms introduced in the last sections, the core application being the solar cadaster of Geneva that was built in several steps from 2011 to 2016.

Solar Cadaster in Geneva's Building Roofs

Context and Additional Methodological Issues

The solar cadaster of the Canton of Geneva was implemented in collaboration between different academic partners: hepia, EPFL

and Politecnico of Milano (Desthieux et al., 2011), using the above methods and algorithms. The Canton of Geneva totalizes an area of about 300 km². Such a large area involves to: (i) divide the DSM of Canton of Geneva into about 55 tiles of 3 km × 3 km (**Figure 5** top), (ii) compute solar radiation for each tile separately, and (iii) to merge results by tiles on the

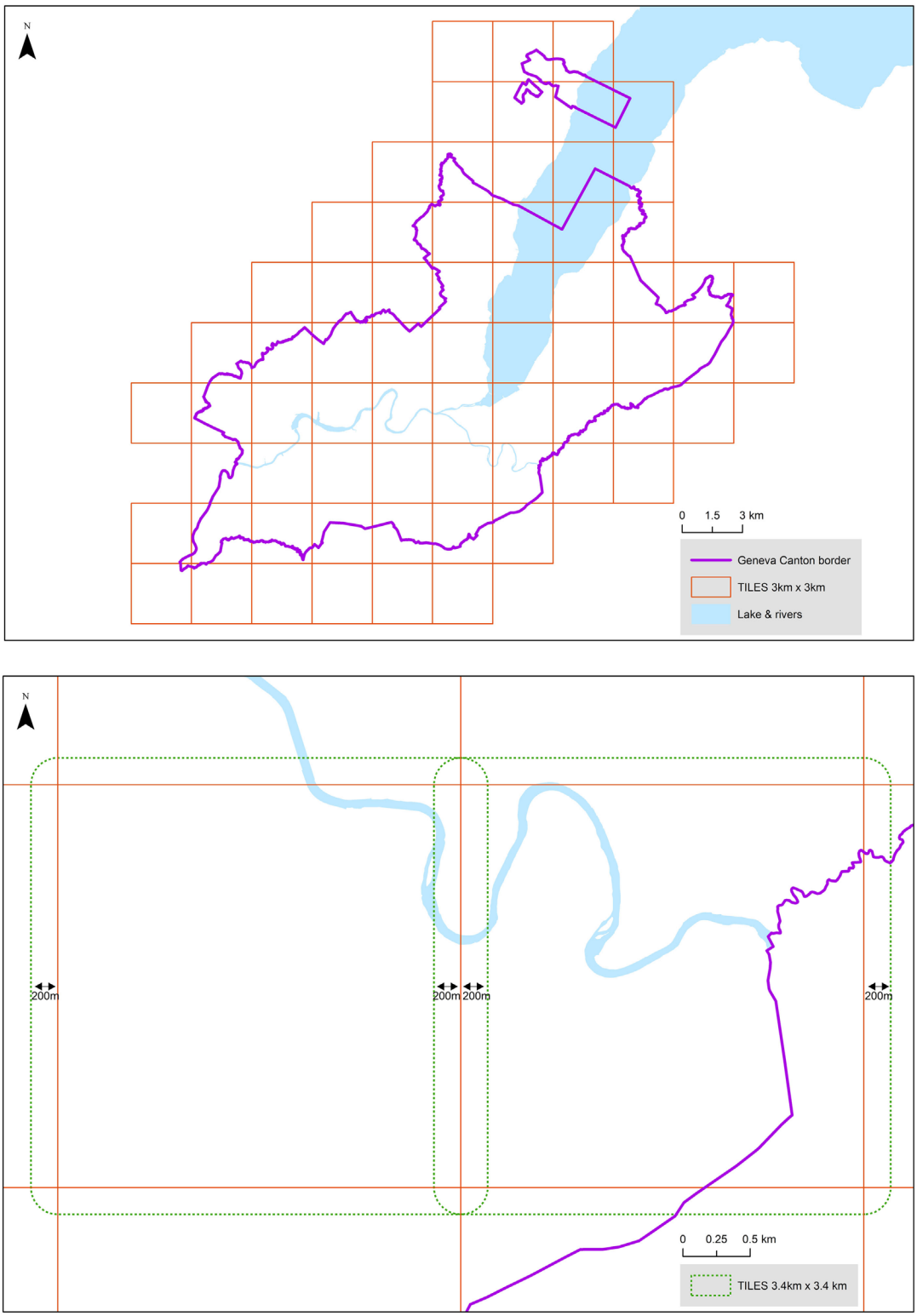

FIGURE 5 | Splitting the Canton of Geneva in tiles of 3 km × 3 km (top); adding a buffer of 200 m to each tile avoiding possible mutual shadowing effects (bottom).

whole Canton. The size of tiles includes an additional length of 200 m from each side in order to avoid possible mutual shadowing effects from one tile to another (particularly important to consider in urban areas with tall buildings). Therefore, final tiles used for computation have a dimension of 3.4 km × 3.4 km (**Figure 5** bottom).

Moreover, the Canton of Geneva, whose altitude ranks from 372 to 500 m, is surrounded by mountains: on the North and West sides ("Jura," top at 1,700 m), South ("Salève," top at 1,300 m) and East ("Voirons," top at 1,400 m), as showed in **Figure 6**. They may create additional shadowing effects depending on the time of the day and the season. Such shadowing effects should be considered in addition to those created by close built environment. The reference meteorological station (Geneva Airport) considered by METENORM takes into account few or very partially such shadowing effects, being located in the middle between all these mountains. Therefore, SVF and hourly shadowing on beam component should be also casted on the agglomeration of Geneva including surrounding mountains. This shadow casting is done in one-step (without tiling) using the DTM at low resolution (50 m × 50 m), thus allowing to save computation time. Then, outputs are clipped by tile and compared to those obtained from DSM at the tile's scale according to Eq. 8 given below.

At every hour, any DSM pixel in Geneva is shadowed if one of those shadows on beam components resulting from close environment (DSM) or relief (DTM) are equal to 0. The minimum SVF value between DSM and relief is then considered. Therefore, this methodological approach was selected for a global shadowing analysis at the scale of the Canton of Geneva.[1]

[1] Ideally, SVF should be computed on a global horizon that integrates both obstacles from close environment (buildings, trees, etc.), as given by the DSM and from relief as given by the DTM. It would mean to compute the area of Geneva in one-step based on a DSM at high resolution at the scale of the whole agglomeration without tiling, unhappily totally prohibitive in terms of computation time.

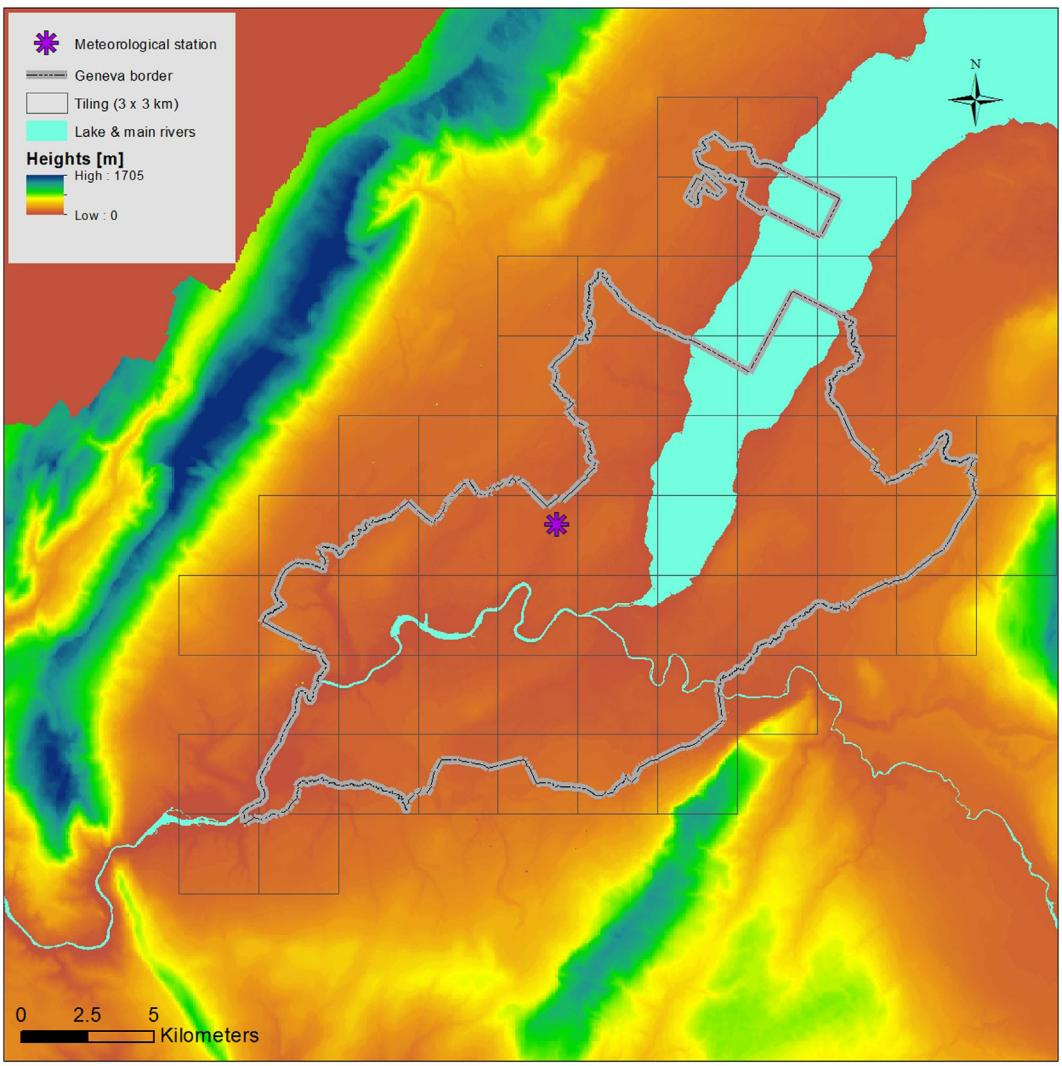

FIGURE 6 | Agglomeration of Geneva highlighting the relief, the meteorological reference station, and the tiling grid.

Equation 7 (see Final Irradiation Formula Applying Shadowing Factors to Solar Components) should be thus adapted in the following way:

$$I_{g\beta\gamma} = \underbrace{I_{b\beta\gamma} r_b S_{b,DSM} S_{b,R}}_{\text{Beam}} + \underbrace{I_{dh}\left\{\frac{I_g - I_d}{I_0} r_b S_{b,DSM} S_{b,R} + \min(SVF_{DSM}, SVF_R)\left[1 - \frac{I_g - I_d}{I_0}\right]\right\}}_{\text{Diffuse}} + \underbrace{0.5 I_g a (1 - \cos\beta)}_{\text{Reflected}}, \quad (8)$$

with:

$S_{bh,DSM}$: shadowing effect from close environment (computed on DSM)on beam and diffuse circumsolar component {0,1}.
$S_{bh,R}$: shadowing effect from relief (computed on DTM) on beam and diffuse circumsolar component {0,1}.
SVF_{DSM}: SVF computed on DSM (close environment) [0, 1].
SVF_R: SVF computed DTM (relief) [0, 1].

Implementation of Geneva's Solar Cadaster

The solar cadaster of Geneva was developed and updated in three steps:

1. In 2011, the raw solar irradiation (monthly and yearly) was processed for each pixel (0.5 m × 0.5 m of resolution) of the Geneva DSM based on LiDAR data acquired in 2009. Average irradiation value was calculated by building roof piece, in order to rank their potential for solar radiation.
2. In 2014, more sound indicators were added in the perspective of active solar energy use. Suitable roof areas for solar panels were identified by selecting yearly irradiation pixel with more than 1,000 kWh/m²/year. Such a threshold empirically allows to take into account low shaded areas and orientations from 40° (slightly North-East) to 275° (slightly North-West). Different indicators, such as the solar energy production, economic (cost of investments, annual costs, subsidies), and environmental (CO_2 saved emission), were computed for these suitable roof areas.
3. In 2016, the full solar cadaster was updated based on the following elements: (i) new LiDAR dataset acquired in 2013, (ii) improved solar algorithms as those presented in Section "Methodological Framework," and (iii) improved calculating capacity using cloud computing (see Cloud Computing).

The solar cadaster of Geneva was made available by means of:

1. The Geneva Geoportail (SITG)/Energy section developed and implemented for professional users (energy planners and engineers, State administration). This Geoportail allows users to download solar radiation open data at different scales (raster pixel, suitable roof area, whole roof element and whole building, district and municipality). Later on, this type of data can be used for different purposes, such as: (i) GIS spatial analysis, (ii) solar energy planning (**Figure 7**).

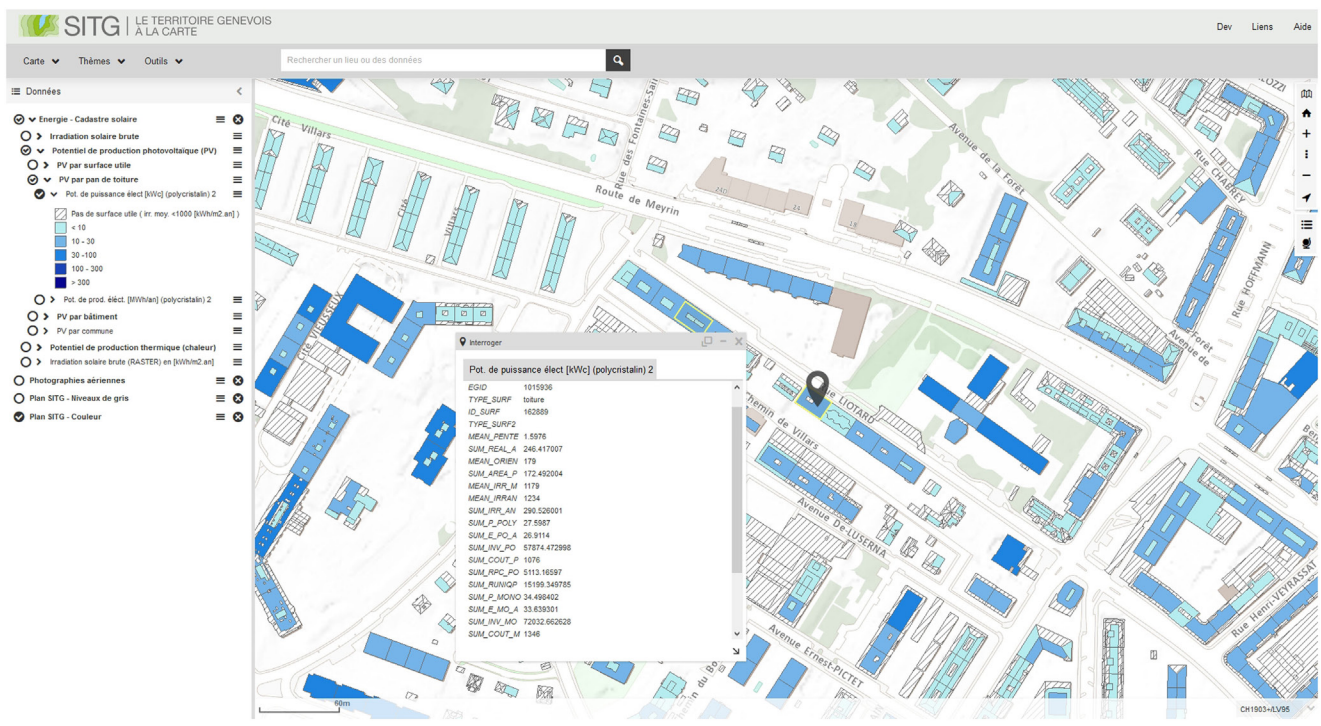

FIGURE 7 | Geneva Geoportal and specific section dedicated to solar cadaster layers. Reproduced from SITG—https://www.etat.ge.ch/geoportail/pro/?mapresources=ENERGIE_SOLAIRE (2017). No permission is required from the copyright holder for the use of this image in this manuscript.

2. The public interface developed and implemented for the wide citizen. It contains the same raw data of Geneva Geoportail (SITG), but displays them in a more friendly way. A main goal of this public interface is to promote solar installations in built areas as a major lever for energy transition (**Figure 8**), thus raising awareness among private and public entities about the solar energy potential that is available on many Geneva's rooftops.

The implementation of the Geneva's solar cadaster is discussed and presented more in details in Desthieux et al. (2018).

Cloud Computing

The first solar cadaster of 2011 was processed with a single instance machine (32 GB Ram, 2 processors and 8 cores) and using a reduced sky vault of only 137 light sources for SVF purpose. The calculation time for each tile of 3.4 km × 3.4 km was around 40 h (about 20 h for SVF and 20 h for solar radiation including hourly shadowing on beam) with a total of about 2,000 h for the whole Canton of Geneva. This important constraint made impossible any further replication in a similar study. Therefore, in the framework of the Canton of Geneva solar cadaster's update, made in 2016, the code was parallelized on the cloud computing's infrastructure of hepia (24 instances containing each one 2 processors). Using the sky vault of 580 light sources (instead of 137 as used in 2011) for SVF calculation, resulted in about 16 h of calculation time for each tile (12 h for SVF and 4 h for hourly shadowing on beam and global solar radiation). Hence, about 900 h of calculation time were needed to process the whole Canton of Geneva, which is a significant improvement when compared to the calculation time (2,000 h) needed in 2011. For more details about cloud computing infrastructure and capabilities, the reader can refer to Boulmier et al. (2016a,b).

Finally, it is also worth mentioning that using GPU (Graphics Processing Unit) technology, particularly suitable with the matrix approach of shadow casting proposed by Ratti and Richens (1999), allows a much more significant reduction on computing time. In particular, it will enable to extend the solar cadaster to the whole Swiss-French transborder agglomeration of Geneva (2,000 km^2), still preserving the use of a high resolution (0.5 m × 0.5 m) DSM for solar irradiation analysis.

Solar Radiation Analysis on Facades

So far, no solar cadaster on building facades has been made in the Canton of Geneva. Nevertheless, hepia's model introduced in this paper is ready to be used for this purpose. It is worth mentioning that due to different buildings' topology, a full cover of the Canton with such a cadaster is not considered relevant. Hence, specific and appropriate areas should be first targeted. Indeed, the use of already built building facades for active solar energy purpose is not as systematic as for roofs, as only some elements of facades, like balconies, may remain available. In general, industrial areas offer more and better opportunities for solar panel installation on facades.

The following figure highlight solar radiation outputs calculated for two case-study areas of Geneva, both characterized by relatively tall buildings with rectangular forms: (i) existing buildings belonging to the neighborhood of "Meyrin Cité," built during the 1960's (**Figure 9**), (ii) a recent project mixing a new

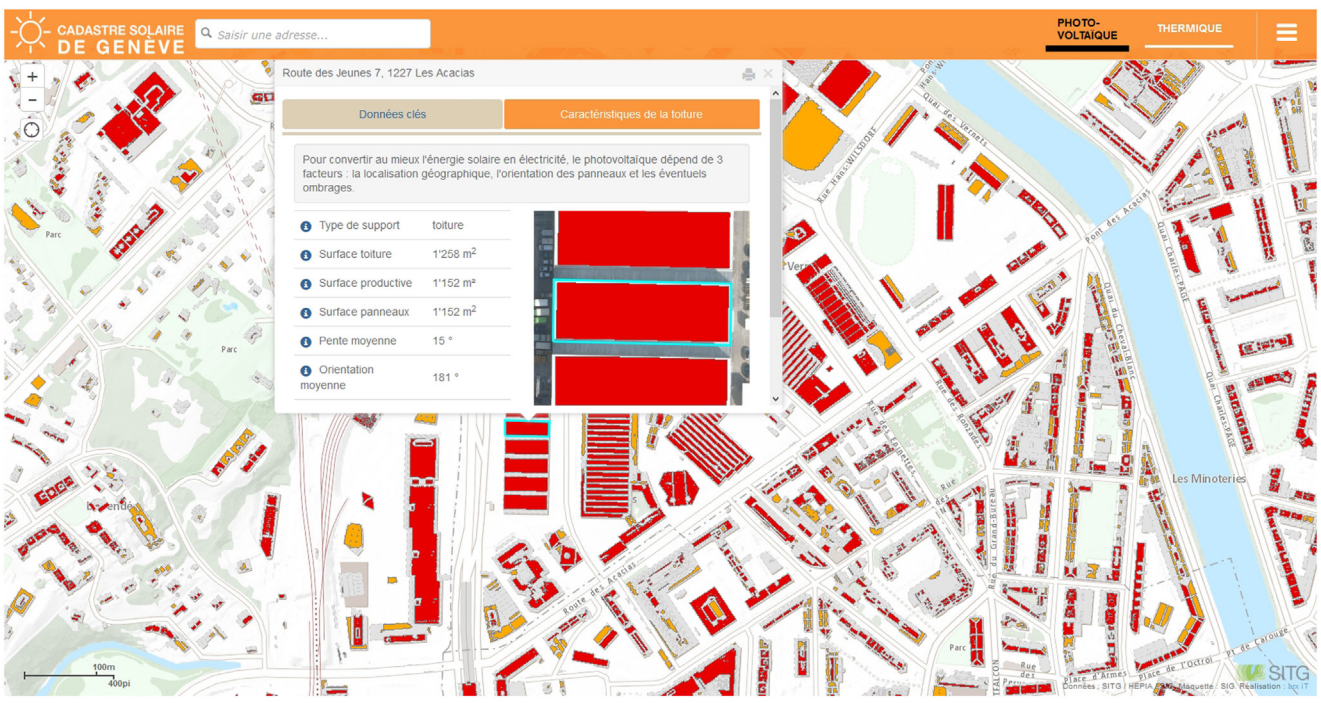

FIGURE 8 | Web-based tool developped by arx it under mandate of SITG; example of display for main rooftop characteristics. Reproduced from SITG—https://sitg-lab.ch/solaire (2017). No permission is required from the copyright holder for the use of this image in this manuscript.

set of buildings and existing industrial areas belonging to the neighborhood of "Carouge" (**Figure 10**). The latter emphasizes the interest of this tool to model solar irradiation facade access for a new set of buildings to be constructed.

VALIDATION OF THE METHODS AND ALGORITHMS

This section shows the results of comparison between hepia's SVF and global irradiation models (with variations on sky vault density) and other models and measurements in some case-study areas in Geneva. The validation process distinguishes the cases of horizontal or titled surfaces and vertical surfaces (facades).

Validation on Horizontal and Titled Surfaces in Geneva

Methodological Background of the Validation Work

In the framework of Geneva's solar cadaster developed in 2011, a validation of SVF and irradiation results was carried out by the University of Geneva (Ineichen, 2012) in two distinct areas of

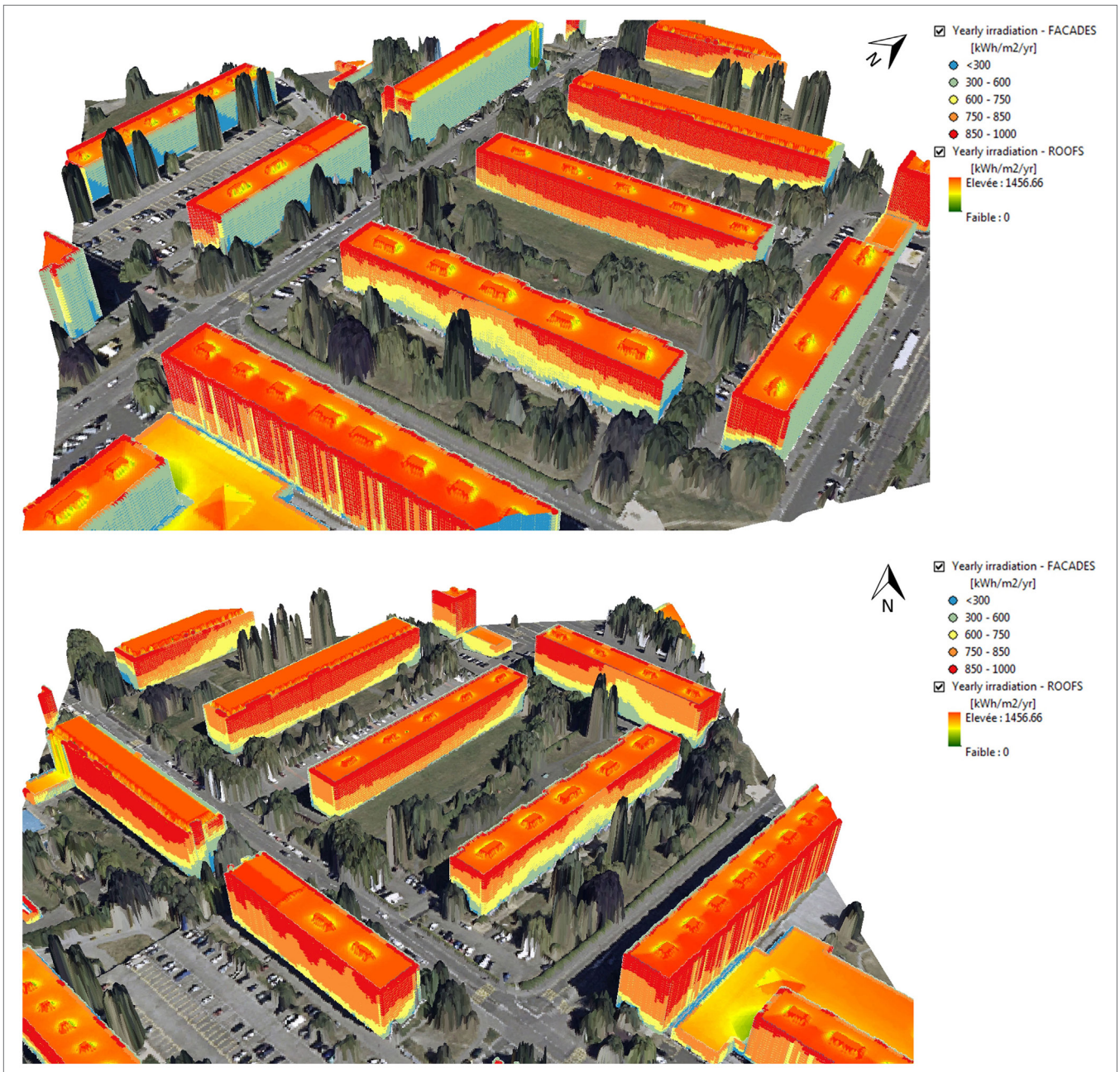

FIGURE 9 | 3D representations of the solar radiation outputs (in kWh/m²/year) on existing building facades and roofs in the "Meyrin Cité" neighborhood (Geneva), showing two different expositions; adapted with permission from ©2016 IEEE (Boulmier et al., 2016a,b).

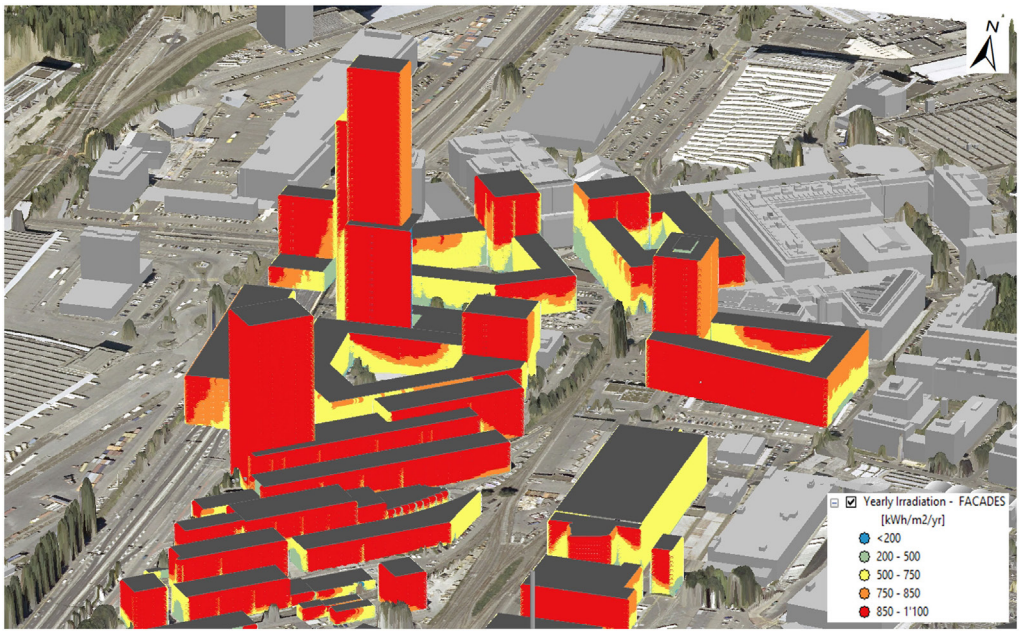

FIGURE 10 | 3D representation of the solar radiation outputs (intensity in kWh/m²/year) on building facades in a sector of the Municipality of Carouge, mixing new tall building developments and existing industrial areas.

Geneva: "Jonction" and "Unimail," as introduced in **Figure 11**. The main goal was to validate if hepia's approach (based on the algorithms presented in Section "Methodological Framework") gave results similar to those from UNIGE's approach, which was based on local data input (fisheye catchment for modeling horizon and local meteorological data). If positive, this would validate hepia's model for processing solar radiation on large urban areas trough: (i) an automated and systematic way, (ii) a good level of accuracy and reliability. As introduced in the present paper, since 2011 this initial comparison and validation has been enriched with the new developments brought to the hepia's model.

The validation made in the area of "Jonction" aimed to compare SVF and irradiation values on horizontal surfaces considering different situations of shadowing: point 1 on the top of a tall building free of shadowing from surrounding environment, points 2, 5, and 6 in the buildings' courtyard. The validation made in the area of "Unimail" aimed to compare SVF and irradiation values on titled surfaces (roof of the University building) almost free of shadowing from surrounding environment (slope = 17° for all points, and aspect = 40° for points *c* and *d*, 220° for *a* and *b*, 0° and 360° being North).

Also in 2011, the University of Geneva made fisheye catchments for all studied locations (**Figure 12**), thus allowing to model the 360° horizon from each point and to calculate SVF and solar irradiations from such catchments. In hepia's model, horizons were generated from DSM constructed from 2009 LiDAR data. As already mentioned in Section "Application of Shadow Casting to Solar Diffuse Component (SVF) and Choice of an Appropriate Sky Vault Model," the use of such data involves take into account irregularities in the height of DSM (caused by LiDAR interpolation on each pixel), which may lead to micro-shadowing effects between neighbor pixels.

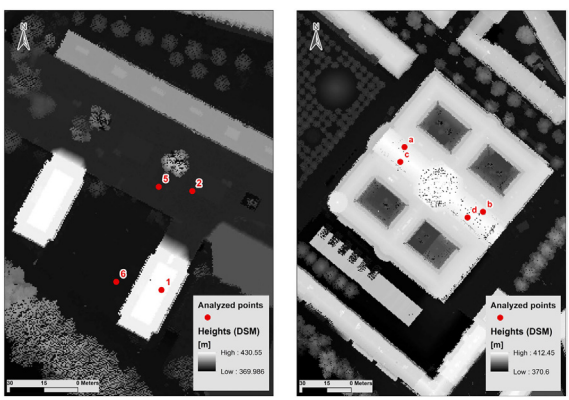

FIGURE 11 | Studied areas in Jonction (left hand-side image) and Unimail (right hand-side image) with location of points used for comparison.

In "Unimail" area, the DSM created from LIDAR resulted in significant variation in aspect, slope from one point of the roof (pixel) to another, also impacting SVF and irradiation outputs. Therefore, average values were calculated inside a 1-m buffer around each point. For instance, inside these buffers standard deviation was around 65 kWh/m²/year for irradiation values, which is considered significant.

The different sky models used for SVF calculation and considered for the comparison study are presented as follows:

- 1,297 solid angles with equal size of 5 msr isotropically distributed over the sky vault (reference model of UNIGE).
- 580 solid angles with equal size of 20 msr (reference model of hepia in 2016).
- 145 solid angles with equal size of 40 msr (Tregenza's model).
- 137 solid angles with equal size of 40 msr, similar to Tregenza's model, but starting at 14° in height in order to attenuate LIDAR's micro-shadowing effect (reference model initially used by hepia during the solar cadaster of 2011).
- 400 solid angles with an equal-angular distribution (8° in azimuth and 7° in height), thus involving a densification of points toward zenith.

Weighting factor based on the sinus of light source's height was applied to the sky models (as exposed in Eq. 3), except for the models with 137 (in accordance with the SVF calculated in 2011) and 400 light sources (indirect weighting factor due to densification toward zenith).

Concerning irradiation calculation, both models used meteorological data (Gh, Dh) from former version of Meteonorm v6.1 (used during the solar cadaster implementation of 2011). As already mentioned in Section "Meteorological Data Sources," hepia's model used Hay's diffuse irradiation model and average hourly irradiation values by month. For sensitivity analysis purpose, comparisons were made in UNIGE's model between Perez's and Hay's diffuse models of transposition, and between hourly and average hourly values by month.

In **Table 1**, SVF and yearly radiation results from hepia are compared to the values obtained by the University of Geneva (UNIGE model).

Discussion of the SVF Validation's Results

Related to the comparison between different models used for SVF calculation (**Table 1**), the following comments are worth mentioning:

- Among the different sky models used, results based on hepia's reference sky model (580 light sources) globally shows the closest values against those of UNIGE considering the sky model of 1,297 light sources. Slightly negative difference (hepia—UNIGE) can be explained by neighborhood micro-shadowing effects caused by LiDAR interpolation in each pixel, even if such effects are reduced due the low weight given to the sky points close to the horizon.
- Former sky model with 137 light sources without sinus weighting factor used in the first Geneva's solar cadaster of 2011 gives significantly underestimated SVF values; hence, the improvements brought to algorithms applied during the update of Geneva's solar cadaster in 2016.
- Few differences between the dense sky models (580 and 1,297 light sources) and the lower one (145 light sources) are worth mentioning, which makes the latter acceptable to be used in SVF calculation for large urban areas. Main goal is to save computing time (factor of 2.5 when compared with the model of 580 light sources).
- Using the equal angular 400 light sources' model tends to overestimate SVF, as the number of light sources toward the zenith are too high.
- In hepia's model, SVF values slightly decrease when using 1,297 light sources instead of 580. This is probably due to the increasing number of light sources not visible from the points taken into analysis.
- Using DSM from LIDAR in inclined surface like in Unimail area and averaging values in 1 m buffers around studied points lead to relatively significant lower outputs (about −8%) due to high variation in slope and aspect. However, outputs are very similar if only representative pixels of the slope (17°) and aspects (220° for south-west) of the roof are taken into account.

In conclusion and to sum up, this comparative study between hepia's and UNIGE's models allowed comparing SVF calculation

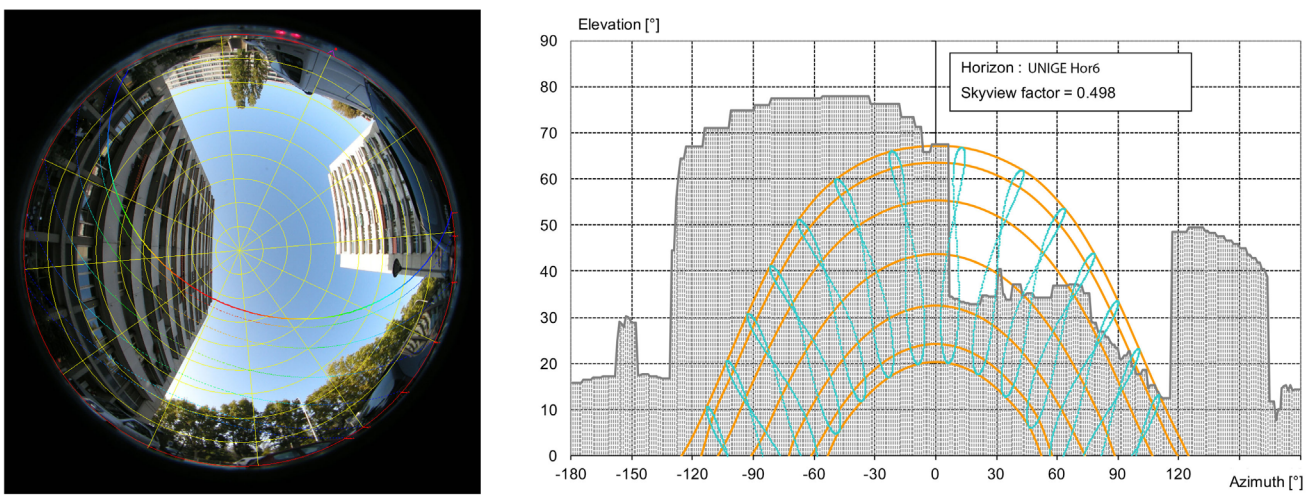

FIGURE 12 | Illustration of the construction of the horizon from fisheye catchment in point 6: image of the circular stereographic projection (left) and projection into Cartesian coordinate system (right). Reproduced from Ineichen (2012). No permission is required from the copyright holder for the use of this image in this manuscript.

TABLE 1 | Comparison on sky view factor (SVF) values (at the top) and irradiation values I_g on horizontal (Jonction) and inclined (Unimail) surfaces (in kWh/m^2/year) (at the bottom) for both studied areas (Jonction and Unimail) between "U"—UNIGE's model using fisheye catchment and "H"—hepia's model using the digital surface model from LIDAR.

SVF

			HEPIA					UNIGE		Comparison						
	Point ID	**Type**	**SVF 137**	**SVF 145**	**SVF 400**	**SVF 580**	**SVF 1297**	**SVF 145**	**SVF 1297**	**H137/ U145**	**H137/ U1297**	**H145/ U145**	**H145/ H580**	**H400/ U1297**	**H580/ U1297**	**H1297/ U1297**
Jonction	1	Top of roof	1.000	0.999	1.000	1.000	0.997	0.997	0.995	1.00	1.01	1.00	1.00	1.01	1.01	1.00
	2	Courtyard	0.588	0.678	0.730	0.685	0.675	0.673	0.689	0.87	0.85	1.01	0.99	1.06	0.99	0.98
	5	Courtyard	0.544	0.652	0.700	0.684	0.669	0.675	0.688	0.81	0.79	0.97	0.95	1.02	0.99	0.97
	6	Bottom of building	0.346	0.480	0.533	0.488	0.480	0.49	0.498	0.71	0.69	0.98	0.98	1.07	0.98	0.96
Unimail	b	North-East titled roof	0.859	0.911	0.960	0.920	0.915	–	0.969	–	0.89	–	0.99	0.99	0.95	0.94
	d	South-West titled roof	0.830	0.891	0.950	0.900	0.890	–	0.969	–	0.86	–	0.99	0.98	0.93	0.92

Irradiation

			HEPIA					UNIGE		Comparison						
	Point ID	**Type**	**I_g(137)**	**I_g(145)**	**I_g(400)**	**I_g(580)**	**I_g(1297)**	**I_g(145)**	**I_g(1297)**	**H137/ U145**	**H137/ U1297**	**H145/ U145**	**H145/ U1297**	**H400/ U1297**	**H580/ U1297**	**H1297/ U1297**
Jonction	1	Top of roof	1,207	1,207	1,207	1,207	1,206	*Not analyzed*	1,201	*Not analyzed*	1.00	*Not analyzed*	1.00	1.01	1.01	1.00
	2	Courtyard	854	888	970	891	887		895		0.95		0.99	1.08	1.00	0.99
	5	Courtyard	773	830	959	841	838		866		0.89		0.96	1.11	0.97	0.97
	6	Bottom of building	348	460	483	464	460		507		0.69		0.91	0.95	0.92	0.91
Unimail	b	North-East titled roof	954	979	1,002	983	981		1,058		0.90		0.92	0.95	0.93	0.93
	d	South-West titled roof	1,174	1,203	1,229	1,206	1,203		1,304		0.90		0.92	0.94	0.92	0.92

using: (i) DSM from LIDAR with fisheye catchment for urban environment modeling, (ii) different sky models. If DSM derived from LIDAR data is used, a sky model with 580 light sources seems to be a good compromise between the density of light sources in the sky vault and the most accurate possible SVF outputs. Nevertheless, the sky model with 145 light sources also gives satisfying results, especially when processing solar cadasters in large urban areas, thus allowing to save computation time.

Discussion of the Solar Irradiation Validation's Results

Differences between hepia and UNIGE results are: (i) globally low, (ii) proportionally similar when comparing both SVF outcomes (**Table 2**).

With regard to the comparative study made in 2011 using the same values from UNIGE, recent developments made in the hepia's model enabled to reach much closer results. This is particularly the case for point #5 (hepia 580/UNIGE 1297 = 97% instead of 89% with the 137 model of 2011) and point #6 (hepia 580/UNIGE 1297 = 97% instead of 69% with the 137 model of 2011), both surrounded by obstacles, thus being significantly shadowed.

Comparison on Unimail's titled roof also emphasizes that using DSM based on LIDAR data creates the foregoing mentioned micro-shadowing effects (Section "Application of Shadow Casting to Solar Diffuse Component (SVF) and Choice of an Appropriate Sky Vault Model"), hence resulting in decreasing irradiations values (about −7%) relatively to those of UNIGE or Hepia.

Two types of sensitivity analysis were made in order to validate the suitability of using average hourly irradiation values derived from the Hay model, presented as follows. Considering the sensitivity analysis on using real hourly or average hourly irradiation values by month, differences are very low for the UNIGE's model: almost 0% for the yearly global irradiance, with a maximum dispersion of 2% for the monthly global irradiance (**Figure 13** at the top), and 4% for the monthly diffuse irradiance (**Figure 13** at the bottom).

A similar sensitivity analysis for inclined studied points of Unimail was made in order to compare the transposition models of Perez (with hourly irradiation values) and Hay (with average hourly values by month). Results show global differences of 1% on the global component and 2% on the diffuse component, with monthly dispersion of 2% for global and 4% for diffuse components. Such differences would be slightly lower if hourly irradiation values of Hay's model were used instead (Ineichen, 2012).

In conclusion and to sum up, this comparative study highlights again that the sky model with 580 points is the best compromise when processing DSM based on LIDAR data for horizontal and titled (not vertical) surfaces. The sensitivity analysis also underlines that using the average hourly irradiation values by month (more suitable for processing large areas) derived from the transposition model of Hay gives low and acceptable differences when compared to the hourly values inferred from the transposition model of Perez's. Finally, it is worth mentioning that this result is particularly relevant on a yearly balance.

Validation on Vertical Surfaces with PVSyst

Methodological Background of the Validation Work

A comparative study was made in collaboration with the HESSO-Wallis for the case-study area presented in Section "Solar Radiation Analysis on Facades" (Geneva/Meyrin). In this case, results of irradiation on facades from hepia and PVSyst modeling were compared for three selected facade points, each of them presenting different heights. The location of the studied points and the PVSyst built environment models are shown in **Figure 14** (same area as displayed in **Figure 9**).

As the used version of PVSyst (6.5.3) does not process DSM, surrounding environment of each point was manually modeled to be as similar as possible to the DSM (**Figure 15**).

The main characteristics of each point are presented as follows:

1. point located in the corner between the main facade and an external chimney;
2. facade in front of a big tree, which is about 28 m higher than the top of the building;
3. facade with middle level of obstruction (tree and frontal building).

TABLE 2 | Results of comparison of global radiation values in the collector plane (in kWh/m²/year) between the solar model described in this work (hepia) and the simulation using PVsyst (HESSO-Valais) with and without trees' consideration. The height values are given with respect to the building ground level.

		Global radiation (kWh/m²/year)							
		WITH tree		NO tree (reference)		Tree shadowing effect		Diff. HEPIA-PVsyst	
	Height (m)	PVSyst	HEPIA	PVSyst	HEPIA	PVSyst (%)	HEPIA (%)	With trees (%)	No trees (%)
Point 1	20.8	638	578	638	578	0	0	−10	−10
	14.8	567	427	630	543	−10	−21	−33	−16
	9.8	322	237	601	480	−46	−51	−36	−25
Point 2	19.9	694	744	788	862	−12	−14	7	9
	14.9	629	683	788	862	−20	−21	8	9
	9.9	559	610	780	846	−28	−28	8	8
Point 3	17.7	811	834	811	835	0	0	3	3
	12.7	772	780	781	797	−1	−2	1	2
	7.7	725	738	759	767	−4	−4	2	1

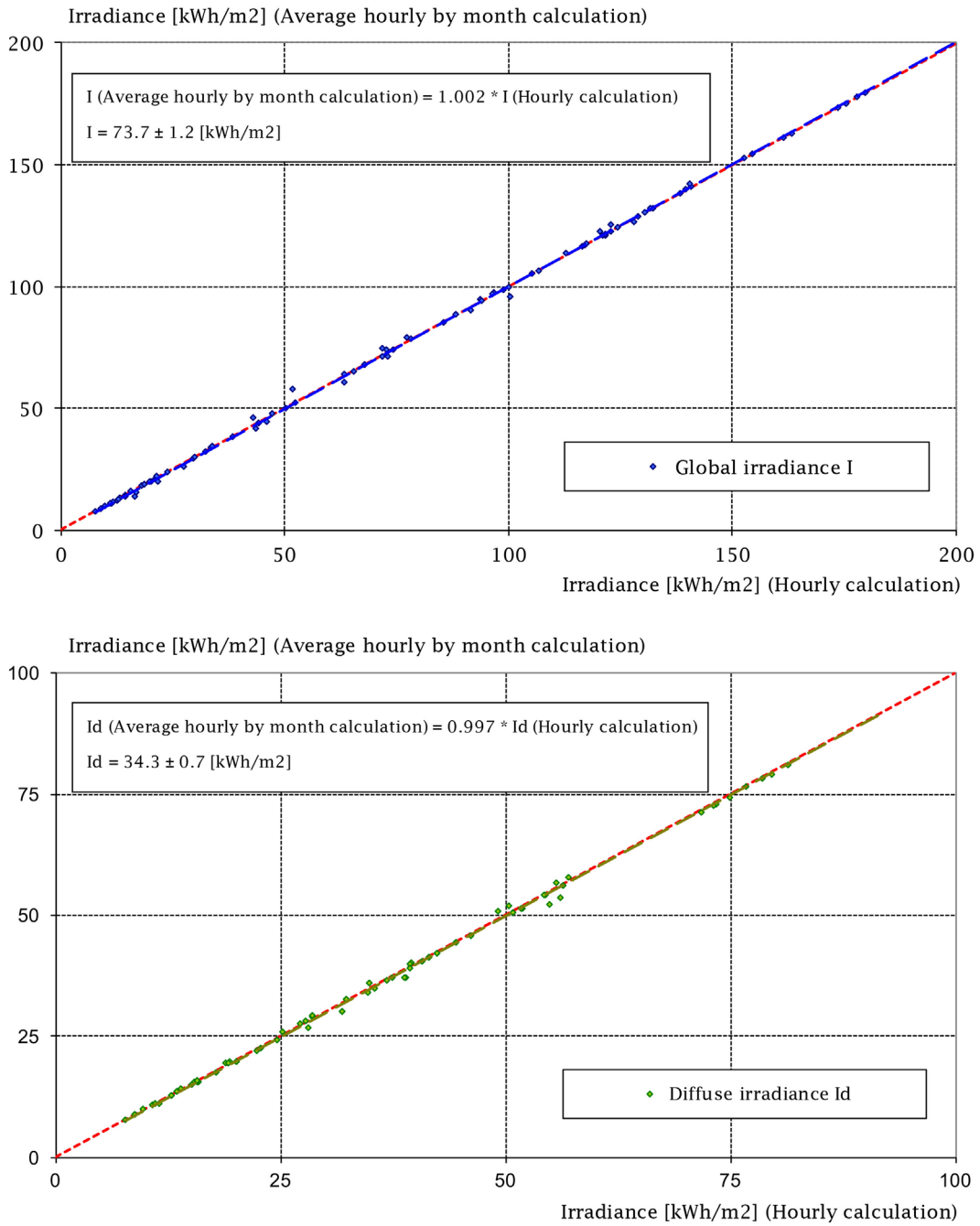

FIGURE 13 | Comparison of results obtained by the UNIGE's on all studied points with real hourly and average hourly by month irradiance values, on a monthly base and distinguishing global (top) and diffuse (bottom) components. Reproduced from Ineichen (2012). No permission is required from the copyright holder for the use of this image in this manuscript.

Using PVSyst and Hepia models, yearly global irradiation was simulated for each of these three locations (points at different heights) (**Table 2**). Both models use: (i) the same meteorological data input (Meteonorm® version 7.1, station: Genève-Cointrin), (ii) the Hay diffuse model, and (iii) an albedo factor of 0.13 for the reflected component. Hourly values of global and diffuse horizontal irradiation, ambient temperature, and wind velocity were imported in PVSyst model. From these data PVSyst computes: (i) the horizontal and normal beam irradiation, (ii) the global irradiation on tilted plan, and (iii) a clearness index, which is the ratio between the horizontal global irradiance and the irradiance available out of the atmosphere. Indeed, these data are necessary to perform a simulation with PVsyst. On the other hand, hepia's model only used the

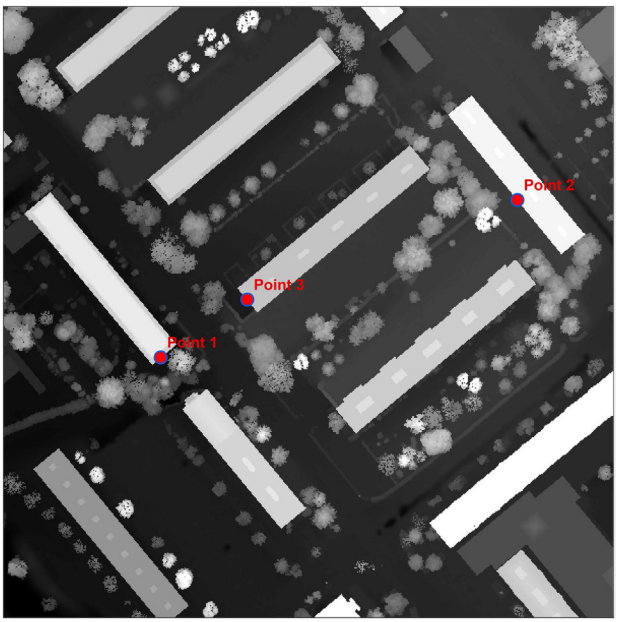

FIGURE 14 | Location of the three points tested in the case-study area of Geneva/Meyrin.

diffuse and horizontal radiation from Meteonorm® as input. Comparison is made with and without considering trees in the respective 3D models (DSM and the model built manually in PVSyst) of the built area, thus emphasizing their effect.

Discussion of the Validation's Results

The following comments can be made with regard to the comparison shown in **Table 2**:

- The difference of values between hepia and PVSyst (processed by HES-VS) is mostly explained by the way the built environment was modeled (neighbor trees and buildings). This can be observed in part through the shadow caused by trees (by calculating the ratio "*no tree*"/"*with* trees"). The impact is higher with hepia's model based on DSM than with PVSyst; hence, values from hepia are globally lower.
- Outputs from hepia and HES-VS area are globally convergent for points #2 and #3. This convergence is particularly significant for point #3, for which trees are less influent and surrounded built area is much easier to model in PVSyst.
- In contrary, divergences are much higher for point #1, which is more shaded by surrounded built environment (trees and building details like a chimney). Moreover, surrounded built environment around this point is more complex to model in PVSyst. Such divergences can be also explained by the fact that hepia's model based on DSM underestimates the reflected component of the solar irradiation, which becomes very influent in vertical facades and when parts of facades face to each other like in spot 1.
- Finally, it is worth mentioning that a previous comparison was made with the model of hepia without including the weighting factor in SVF calculation for facades, as defined in Eq. 3 (see Application of Shadow Casting to Solar Beam Component). Indeed, results were more divergent from those of PVSyst (improvement of about 5%).

In conclusion and to sum up, differences remain relatively low in some points (#2 and #3), which attests that hepia's model is totally reliable; especially after weighing factor was introduced in SVF calculation. Moreover, PVSyst updated version will be released soon. A major improvement of this new version of PVSyst is that it will be possible to process more easily imported DSM, thus enabling to improve this comparative study.

CONCLUSION

This article has presented a complete method and tools (hepia's model) used to analyze solar radiation on existing horizontal surfaces, titled roofs, and building facades of the built environment. More particularly, it implements automated processes based on 2D vector-based data (building footprints), 3D vector-based data (roof footprints), and 2.5D data (DSM,DTM).

Concerning the facade component, using such 2D and 2.5D data enables: (i) to deal with the third dimension by generating hyperpoints from the top of building to the ground, (ii) to compute solar radiation on each hyperpoint of the facade. Indeed, such a pseudo 3D approach is sufficient for the solar radiation analysis purpose applied for large urban scales. However, the level of detail is very poor when it is matter of considering some details of the facade, such as balconies and windows. Moreover, there is a major improvement in hepia's model that has to be prioritized during further developments: a better modeling of the radiation reflected component in order to take into account inter-reflections between buildings, which nowadays is extremely complex to automatically process using GIS tools. A reliable solution could be to implement an approach based on the "ray-tracing" concept. Semi-automated image classification should also be implemented in order to detect urban materials and thus deduce albedo factors.

In 2011 hepia's model (limited to solar radiation analysis on building roofs) led to the elaboration of the first version of Geneva's solar cadaster. Since then, many methodological improvements have been brought to hepia's model, predominantly related to the following topics:

- Refinement of the algorithms used for solar radiation calculation. A main focus was given to the reviewing of the sky vault model. Hence, today, in order to calculate a more accurate SVF, hepia's sky vault model uses 580 light sources instead of 137 (as previously used in 2011 for the elaboration of the first version of Geneva's solar cadaster).
- Introduction of weighting factors, which improves SVF modeling.
- Rewriting of the codes in Java (previously written in Matlab) with the support of IT experts. Undoubtedly, Java scrips are more stable and compatible with cloud computing.
- Acceleration of calculation time due to cloud computing solutions implemented through the CTI IceBOUND project.

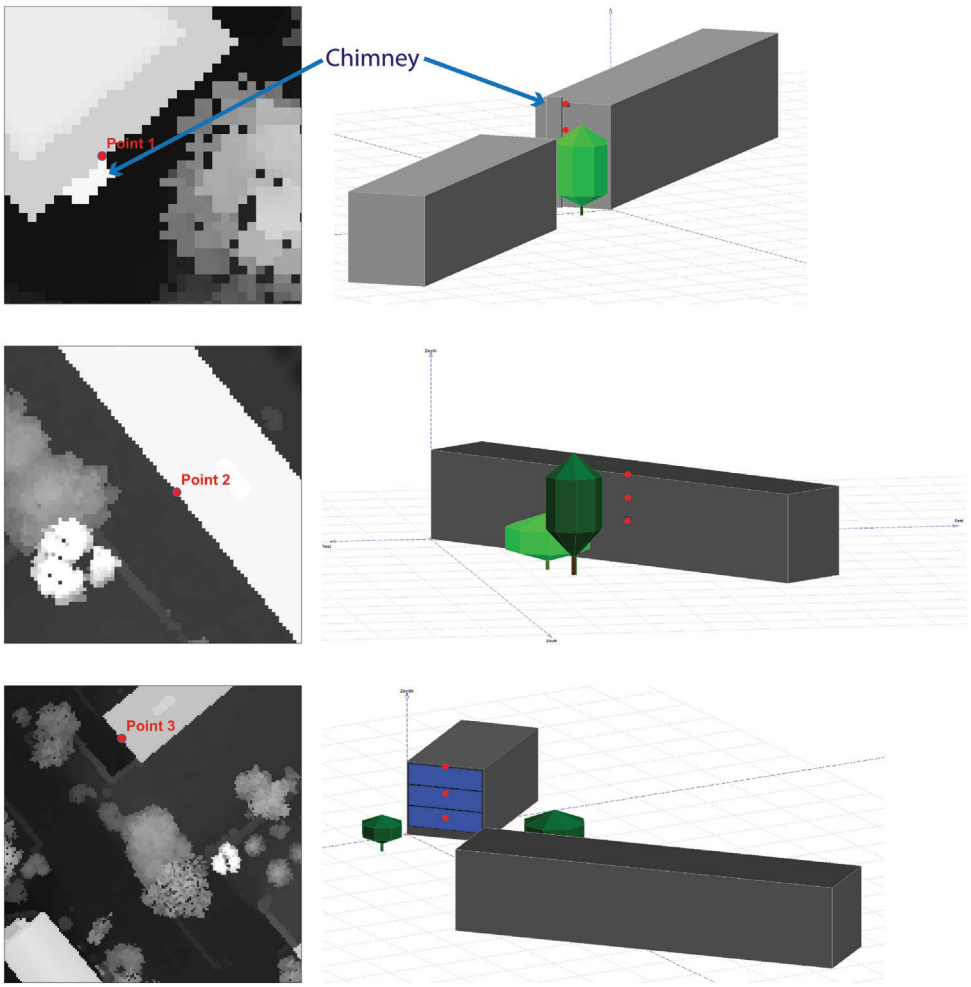

FIGURE 15 | Extracts of the digital surface model (left hand-side images) and 3D modeling with PVSyst (right hand-side images) for the three sets of points tested.

- Addition of the vertical component (facades) to solar radiation calculations. Indeed, when compared to roofs and nearly horizontal surfaces, facades are more demanding and complex to model in 3D. A partial validation of solar radiation calculations was studied for three facades, each of them presenting different heights and particular characteristics on the surrounding built environment. This validation was made through a comparison between shading situations and standard commercially available PV-simulation software (PVSyst).

The good validation results make hepia's model a reliable tool to: (i) automatically process solar cadaster on building rooftops and facades at large urban scales, (ii) support solar energy planning and energy transition policies.

This paper opens up many potential applications from the macro to the micro urban scales:

- At a macro scale, implementation of *enriched urban solar cadasters*, by adding the facade component to the roof components, mainly for urban areas with high potential, such as industries, office buildings, etc. Hence, such a solar cadaster at large urban scale enables better targeting building with high potential for active solar use. Architectural aspects for solar panel integrations should be also taken into account. Therefore, in addition to the demo area (~12 km^2) presented in Section "Applications," other reliable targeted areas for the facade component analysis will be also taken into account for forthcoming updates of Geneva's solar cadaster. Moreover, this tool could be also used to accurately evaluate the potential of building roofs and facades to be constructed, provided that a DSM of such buildings and the surrounding built environment is made available.
- At a middle scale, *modeling of shadowing scenes and solar irradiation at the level of a group of buildings and open spaces/public places*. Main application is in the framework of developing strategies to improve thermal comfort during summer (action related to climate change and subsequent overheating events).
- At a micro-scale, *optimization of energy management and balance at building level*. In this case, the proposed tool enables

to model passive solar energy incoming to roofs and facades, taking into account the shadow effects of the surrounding built environment. Using hourly solar irradiation values would also enable to refine the energy profile of a building.

NOMENCLATURE

DSM	Digital Surface Model
DTM	Digital Terrain Model
SVF	Sky View Factor
$I_{g\beta\gamma}$	Hourly *global* irradiation on the inclined surface (W/h/m^2)
$I_{b\beta\gamma}$	Hourly *beam* or direct irradiation on the inclined surface (W/h/m^2)
I_S	Hourly *diffuse* irradiation on the inclined surface (W/h/m^2)
I_r	Hourly *ground reflected* irradiation on the inclined surface (W/h/m^2)
I_g	Hourly global irradiation on the horizontal surface (W/h/m^2)
I_0	Hourly extraterrestrial irradiation (W/h/m^2)
I_d	Hourly *diffuse* radiation incident on the horizontal surface (W/h/m^2)
γ	Azimuth angle (orientation or aspect) of the inclined surface
β	Slope angle of the inclined surface
S_b	Hourly shadowing effect on beam and diffuse circumsolar components {0,1}
S_d	Shadowing effect on the isotropic part of the diffuse component = SVF [0,1]
l	Any given light source defined by its position (azimuth ψ and height α')
P_0	Any given point (pixel) in the DSM dataset under shadow casting analysis
P_m	Any given point (pixel) in the DSM dataset defined by its position (x, y) and height (z)
S_l(P)	Shadow casted value on P for a given light source l {0,1}
H_{lm}	Height of the line binding the light source l and P_0 at the position of P_m
MSP	Maximum shadow propagation
n	Total number of light sources in the sky vault
α	Height angle of the light source l relatively to the horizontal surface
α'	Height angle of the light source l relatively to the inclined surface defined on P
θ	Angle of incidence of the inclined surface
θ_z	Zenith angle of the light source
ψ	Azimuth angle of the light source
r_b	cosθ/cosθz, transposition factor
A	Albedo coefficient

AUTHOR CONTRIBUTIONS

Introduction, state of the art, methodological framework, overview, and solar irradiation calculation: GD, CC and EM; methodological framework, shadow casting routine: EM, GD, CC, PI, AM, and NA; application: GD, CC, AB, RC and NA; validation and validation on horizontal surfaces/roofs: PI, GD, and CC; validation on vertical surfaces: SD, CE, GD, and CC; and conclusion: GD.

ACKNOWLEDGMENTS

Authors are definitely indebted to all funders and partners that contributed to the development of the proposed approach in the outline of different R&D projects. They would also like to thank Miguel Brito, Cristina Catita, Paula Redweik, and Sara Freitas from the Faculty of Sciences University of Lisbon, for the exchange of ideas and for carrying out some comparative studies in Geneva and Lisbon's spots.

FUNDING

This paper is the result of several research and development activities that were funded in the framework of the following programs and projects: 1. Thematic program in architecture and engineering of the University of Applied Sciences – Western Switzerland (HES-SO)/Topic: Energy District 2050/Project: Urban Sun Skin (USS). Main funder: HES-SO, co-funders: Geneva Energy Agency (OCEN) and Energ company of Geneva (SIG). Amount: 180,000 CHF. 2. Swiss Federal Agency for the Promotion of Innovation Based on Science (CTI[2]), Project ICeBOUND: Cloud Based Design Support System for Urban Numeric Data. Main funder: CTI, cofounders (industrial partners): Geneva Energy Agency (OCEN), Geneva energy company (SIG), Geneva topographic agency (SITG), CERN, arx it. Amount: 336,400 CHF. 3. Solar cadaster of Geneva, carried out in several stages from 2011 to 2016. Funded by: Geneva Energy Agency (OCEN), Geneva energy company (SIG). Amount: 150,000 CHF.

[2]Among other things, CTI aims to bring cutting-edge companies closer to academic research, thus allowing to create a strong dynamic in R&D promotion and to enhance the potential for innovation. Involved partners are Geneva energy agency, Geneva facility agency-SIG, Geneva geomatics agency, Geneva topographic, agency, CTI, Arx iT, HEPIA, CERN, EPFL, and POLIMI.

REFERENCES

Aste, N., Adhikari, R. S., Del Pero, C., and Leonforte, F. (2017). Multi-functional integrated system for energy retrofit of existing buildings: a solution towards nZEB standards. *Energy Proc.* 105, 2811–2817. doi:10.1016/j.egypro.2017.03.608

Axelsson, P. (1999). Processing of laser scanner data – algorithms and applications. *Int. Arch. Photogramm. Remote Sens. Spatial Inf. Sci.* 54, Part 2, 138–147. doi:10.1016/S0924-2716(99)00008-8

Batty, M., and Longley, P. (1994). *Fractal Cities: A Geometry of Form and Function*. London: Academic Press, 394.

Boulmier, A., Abdennadher, N., Desthieux, G., and Carneiro, C. (2016a). *Cloud Based Decision Support System for Urban Numeric Data. Final Report*. Available at: http://lsds.hesge.ch/wp-content/uploads/2016/09/iCeBOUND_Final_Report.pdf

Boulmier, A., White, J., and Abdennadher, N. (2016b). "Toward a cloud based decision support system for solar map generation," in *IEEE 2016 – 8th International Conference on Cloud Computing Technology and Science*, Luxembourg 230–236.

Carneiro, C. (2011). *Extraction of Urban Environmental Quality Indicators using LiDAR-Based Digital Surface Models*. Ph.D. Thesis work, no 5050 EPFL, Lausanne.

Carneiro, C., Morello, E., and Desthieux, G. (2009). "Assessment of solar irradiance on the urban fabric for the production of renewable energy using LIDAR data and image processing techniques," in *Advances in GIS, Proceedings of the 12th AGILE Conference*, eds M. Sester, L. Bernard, and V. Paelke (Berlin, Heidelberg: Springer), 83–112.

Compagnon, R. (2004). Solar and daylight availability in the urban fabric. *Energy Build.* 36, 321–328. doi:10.1016/j.enbuild.2004.01.009

Conseil Fédéral. (2013). *Message relatif au premier paquet de mesures de la Stratégie énergétique 2050 (Révision du droit de l'énergie) et à l'initiative populaire fédérale «Pour la sortie programmée de l'énergie nucléaire (Initiative ‹Sortir du nucléaire›)»*. Bern: Federal Gazette.

Desthieux, G., Camponovo, R., and Gallinelli, P. (2014). *Cadastre solaire du canton de Genève – Phase 2. Analyse du potentiel de production énergétique par les panneaux solaires thermique et PV. Rapport d'étude*. Genève: Office cantonal de l'énergie

(OCEN) et des Services industriels genevois (SIG). Available at: http://ge.ch/geodata/SITG/CATALOGUE/INFORMATIONS_COMPLEMENTAIRES/RAPPORT_CADASTRE_SOLAIRE_PHASE_2_2014.pdf

Desthieux, G., Carneiro, C., and Morello, E. (2011). *Cadastre solaire du canton de Genève. Rapport d'étude*. Genève: Office cantonal de l'énergie (OCEN) et des Services industriels genevois (SIG). Available at: http://ge.ch/geodata/SITG/CATALOGUE/INFORMATIONS_COMPLEMENTAIRES/RAPPORT_CADASTRE_SOLAIRE_PHASE_1_2011.pdf

Desthieux, G., Carneiro, C., Susini, A., Abdennadher, N., Boulmier, A., Dubois, A., et al. (2018). "Solar cadaster of Geneva: a decision support system for sustainable energy management," in *From Science to Society. Progress in IS*, eds B. Otjacques, P. Hitzelberger, S. Naumann, and V. Wohlgemuth (Cham: Springer).

Dubayah, R., and Rich, P. M. (1995). Topographic solar radiation models for GIS. *Int. J. Geograph. Inf. Syst.* 9, 405–419. doi:10.1080/02693799508902046

Erdelyi, R., Wang, Y., Guo, W., Hanna, E., and Colantuono, G. (2014). Three-dimensional SOlar RAdiation Model (SORAM) and its application to 3-D urban planning. *Sol. Energy* 101, 63–73. doi:10.1016/j.solener.2013.12.023

European Commission. (2014). *Communication from the Commission to the European Parliament, the Council, the European Economic and Social Committee and the Committee of the Regions. A Policy Framework for Climate and Energy in the Period from 2020 to 2030*. Bruxelles: COM, 15.

Freitas, S., Catita, C., Redweik, P., and Brito, M. C. (2015). Modelling solar potential in the urban environment: state-of-the-art review. *Renew. Sustain. Energ. Rev.* 41, 915–931. doi:10.1016/j.rser.2014.08.060

Hämmerle, M., Gál, T., Unger, J., and Matzarakis, A. (2011). "Comparison of models calculating the sky view factor used for urban climate investigations," in *Theoretical and Applied Climatology* (Springer-Verlag), 105, 521–527. doi:10.1007/s00704-011-0402-3

Hay, J. E. (1979). Calculation of monthly mean solar radiation for horizontal and inclined surfaces. *Sol. Energy* 23, 301–330. doi:10.1016/0038-092X(79)90123-3

Holmer, B. (2011). "Sky view factors in forest canopies calculated with IDRISI," in *Theoretical and Applied Climatology* (Springer-Verlag), 68, 33–40. doi:10.1007/s007040170051

Ineichen, P. (2012). *Projet Potentiel Solaire 2010. Validation des modèles*. Université de Genève. Available at: http://archive-ouverte.unige.ch/unige:23641

Iqbal, M. (1983). *An Introduction to Solar Radiation*. New York: Academic Press, 390.

Jakubiec, J. A., and Reinhart, C. F. (2013). A method for predicting city-wide electricity gains from photovoltaic panels based on LiDAR and GIS data combined with hourly day simulations. *Sol. Energy* 93, 127–143. doi:10.1016/j.solener.2013.03.022

Kamel, R., Ekrami, N., Dash, P., Fung, A., and Hailu, G. (2015). BIPV/T+ASHP: technologies for NZEBs. *Energy Proc.* 78, 424–429. doi:10.1016/j.egypro.2015.11.687

Klein, S. A. (1977). Calculation of monthly average insolation on tilted surfaces. *Sol. Energy* 19, 325–432. doi:10.1016/0038-092X(77)90001-9

Lindberg, F., Jonsson, P., Honjo, T., and Wästberg, D. (2015). Solar energy on building envelopes – 3D modelling in a 2D environment. *Sol. Energy* 115, 369–378. doi:10.1016/j.solener.2015.03.001

Maleki, S. A. M., Hizam, H., and Gomes, C. (2017). Estimation of hourly, daily and monthly global solar radiation on inclined surfaces: models re-visited. *Energies* 10, 134. doi:10.3390/en10010134

Marszal, A. J., Heiselberg, P., Bourrelle, J. S., Voss, K., and Sartori, I. (2011). Zero Energy Building – a review of definitions and calculation methodologies. *Energy Build.* 43, 971–979. doi:10.1016/j.enbuild.2010.12.022

Miguet, F., and Groleau, D. (2002). A daylight simulation tool for urban and architectural spaces: Application to transmitted direct and diffuse light through glazing. *Build. Environ.* 37, 833–843. doi:10.1016/S0360-1323(02)00049-5

Owen Lewis, J., Ní Hógáin, S., and Borghi, A. (2013). *Cities of Tomorrow – Action Today. URBACT II Capitalisation. Building Energy Efficiency in European cities*. Saint-Denis: Urbact.

Perez, R., Ineichen, P., Seals, R., Michalsky, J. J., and Stewart, R. (1990). Modelling daylight availability and irradiance components from direct and global irradiance. *Sol. Energy* 44, 271–289. doi:10.1016/0038-092X(90)90055-H

Perez, R., Seals, R., Ineichein, P., Stewart, R., and Menicucci, D. (1987). A new simplified version of the perez diffuse irradiance model for tilted surfaces. *Sol. Energy* 39, 221–231. doi:10.1016/S0038-092X(87)80031-2

Perez, R., Stewart, R., Arbogast, R., Seals, J., and Scott, J. (1986). An anisotropic hourly diffuse radiation model for surfaces: description, performance validation, site dependency evaluation. *Sol. Energy* 36, 481–497. doi:10.1016/0038-092X(86)90013-7

Ratti, C., and Richens, P. (1999). "Urban texture analysis with image processing techniques," in *CAAD futures Digital Proceedings*. Atlanta.

Ratti, C., and Richens, P. (2004). Raster analysis of urban form. *Environ. Plan. B* 31, 297–309. doi:10.1068/b2665

Redweik, P., Catita, C., and Brito, M. (2013). Solar energy potential on roofs and facades in an urban landscape. *Sol. Energy* 97, 332–341. doi:10.1016/j.solener.2013.08.036

Ritchie, A., and Randall, T. (2009). Sustainable urban design: an environmental approach. New York: Taylor & Francis, 241.

Robinson, D., Scartezzini, J., Montavon, M., and Compagnon, R. (2005). *Solurban: Solar Utilisation Potential of Urban Sites, Tech. Rep*. Bern: Swiss Federal Office of Energy.

Steyn, D. G. (1980). The calculation of view factors from fisheye-lens photographs, research note. doi:10.1080/07055900.1980.9649091

Teller, J., and Azar, S. (2001). TOWNSCOPE II – a computer system to support solar access decision making. *Sol. Energy* 70, 187–200. doi:10.1016/S0038-092X(00)00097-9

Tregenza, P. R. (1987). Subdivision of the sky hemisphere for luminance measurements. *Light. Res. Technol.* 19, 13–14. doi:10.1177/096032718701900103

Verso, A., Martin, A., Amador, J., and Dominguez, J. (2015). GIS-based method to evaluate the photovoltaic potential in the urban environments: The particular case of Miraflores de la Sierra. *Sol. Energy* 117, 236–245. doi:10.1016/j.solener.2015.04.018

Ward, G. J. (1994). "The RADIANCE lighting simulation and rendering system," in *Proceedings of the 21st Annual Conference on Computer Graphics and Interactive Techniques (SIGGRAPH)* (Orlando, USA).

Conflict of Interest Statement: The authors declare that the research was conducted in the absence of any commercial or financial relationships that could be construed as a potential conflict of interest.